

A STUDY OF TOPOLOGICAL PHASE TRANSITION IN RARE-EARTH MATERIAL YTTRIUM PHOSPHIDE

Thesis submitted

In partial fulfilment of the requirements for the

Degree of

MASTER OF SCIENCE

in

APPLIED PHYSICS

Submitted By:

Anushka Pal

(23/MSCPHY/75)

&

Rashmi Yadav

(23/MSCPHY/73)

Under the supervision of

Dr. Mukhtiyar Singh

(Assistant Professor)



Department of Applied Physics

DELHI TECHNOLOGICAL UNIVERSITY

(Formerly Delhi College of Engineering)

Shahbad Daulatpur, Main Bawana Road, Delhi-110042, India.

June 2025



DELHI TECHNOLOGICAL UNIVERSITY

(Formerly Delhi College of Engineering)

Shahbad Daulatpur, Main Bawana Road,
Delhi-110042

DECLARATION

We hereby certify that the work which is presented in the Research Work entitled "*A study of topological phase transition in rare-earth material Yttrium Phosphide*" in fulfilment of the requirement for the award of the degree of Master in Science and submitted to the Department of Applied Physics, Delhi Technological University, Delhi is an authentic record of our own, carried out during a period from May 2024 to May 2025, under the supervision of **Dr. Mukhtiyar Singh**.

The matter presented in this thesis has not been submitted by us for the award of any other degree of this or any other University. The work has been published in the peer-reviewed journal Physics Letters A with the following details:

Title of the Paper (I): An ab-initio study of structural and topological phase transition in rare-earth yttrium monophosphide.

Author names (in the sequence as per research paper): Anushka Pal, Rashmi Yadav, Ramesh Kumar, Mukhtiyar Singh.

Name of the Journal: Physics Letters A


Status of paper: Published

Date of paper communication: 15 February 2025

Date of paper acceptance: 13 May 2025

Date of paper publication: 28 August 2025


Anushka Pal
(23/MSCPHY/75)



Rashmi Yadav
(23/MSCPHY/73)

SUPERVISOR CERTIFICATE

To the best of my knowledge, the above work has not been submitted in part or full for any Degree or Diploma to this University or elsewhere. I, further certify that the publication and indexing information given by the students is correct.

Place: Delhi

Date: 09/06/2025


Dr. Mukhtiyar Singh
(Supervisor)

ABSTRACT

In this work, we explore the topological quantum phase transitions in Yttrium Phosphide (YP) under varying hydrostatic pressures using *first-principles* calculations based on density functional theory and the Green's function approach. At ambient conditions, YP crystallizes in a rock-salt cubic structure and exhibits metallic character. To examine the pressure-driven behaviour, we studied its structural, mechanical, dynamical, electronic, and topological properties at ambient as well as applied hydrostatic pressure. The compound is found to be both mechanically and dynamically stable, as confirmed by its elastic constants and phonon dispersion curves. A pressure-induced structural phase transition is observed at 63.6 GPa, accompanied by a discontinuity in enthalpy and volume, suggesting a transition from the cubic to a tetragonal structure. The band structure analysis reveals a band inversion near the Fermi level under increasing pressure, a signature of non-trivial topological behaviour. To confirm this transition, we calculated the \mathbb{Z}_2 invariant through the evolution of Wannier charge centers, which confirms a topological phase transition at high pressure. These findings provide valuable insight into the pressure-tuneable topological properties of monophosphides and highlight YP as a promising candidate for future quantum material applications.

ACKNOWLEDGEMENT

We would like to express our sincere gratitude and deep appreciation to our supervisor, **Dr. Mukhtiyar Singh**, Assistant Professor, Department of Applied Physics, Delhi Technological University, for their inspiring guidance, constructive criticism, and valuable suggestions throughout the project. We want to express our gratitude and indebtedness to **Prof. Vinod Singh**, Head of the Department, Applied Physics, Delhi Technological University, for their inspiring guidance.

We would also like to thank **Mr. Ramesh Kumar**, Senior Research Fellow, CQMD Lab, Department of Applied Physics, Delhi Technological University, for his mentorship and for sharing his experience and expertise on this subject. We are thankful for his constant guidance and support. We would also like to thank **Ms. Deepika**, Junior Research Fellow, CQMD lab and our friend **Ms. Sumedha Yadav** for their continuous support and understanding. We would also be thankful to my family and colleagues for their invaluable support, care, and patience during this project.

We would like to acknowledge the National Supercomputing Mission (NSM) for providing computing resources of ‘PARAM Siddhi-AI’, under the National PARAM Supercomputing Facility (NPSF), C-DAC, Pune and supported by the Ministry of Electronics and Information Technology (MeitY) and Department of Science and Technology (DST), Government of India. Lastly, we would like to thank the Department of Applied Physics, Delhi Technological University, for allowing us to work on this topic.

TABLE OF CONTENTS

Contents	Page No.
DECLARATION	ii
SUPERVISOR CERTIFICATE	ii
ABSTRACT	iii
ACKNOWLEDGEMENT	iv
TABLE OF CONTENTS	v
LIST OF TABLES	vii
LIST OF FIGURES	viii
LIST OF SYMBOLS AND ABBREVIATIONS	x
CHAPTER 1 INTRODUCTION	1
1.1 Hall Effect	2
1.2. Topology	4
1.3 Topological Insulator	5
1.4 Topological Semimetals	7
1.4.1 Dirac Semimetal	7
1.4.2 Weyl Semimetal	8
1.4.3 Nodal-Line Semimetal	8
1.4.4 Z_2 Topological Semimetal	9
1.5 Objective	10
1.6 Summary	10
CHAPTER 2 METHODOLOGY	11
2.1. Introduction	11
2.2. Density Functional Theory (DFT)	12
2.3. Exchange correlation functionals	13
2.3.1 Generalized Gradient Approximation(GGA)	13
2.3.1.1 Perdew-Burke-Ernzerhof	13
2.3.2 Hybrid Functional	14
2.4 Computational Packages	14
2.4.1 VASP	14
2.4.2 Wannier90	15
2.4.3 WannierTool	15
2.5 Summary	16
CHAPTER 3 STRUCTURAL AND TOPOLOGICAL PHASE TRANSITIONS IN YTTRIUM MONOPHOSPHIDE	17
3.1 Introduction	17
3.2 Computational details	18
3.3 Structural properties	19
3.4 Stability Analysis	20

3.5 Electronic Structure	22
3.6 Z_2 Topological invariants	25
3.7 Summary	28
CHAPTER 4 CONCLUSION AND FUTURE SCOPE	29
4.1 Conclusion	29
4.2 Future scope	30
REFERENCES	31
PLAGIARISM REPORT	37
PUBLISHED PAPER	40
PROOF AND SCOPUS INDEXING	41
LIST OF CONFERENCE	42

LIST OF TABLES

Table No.	Table Captions	Page No.
3.1	The optimized lattice parameter and structural phase transition (SPT) pressure of YP.	20
3.2	The values of the various elastic properties at applied hydrostatic pressure.	21
3.3	The product of parities of all filled bands at TRIM points in BZ under ambient and exalted pressure values.	26

LIST OF FIGURES

Fig. No.	Figure Captions	Page No.
1.1	Illustration of Hall effects, (a) conventional hall effect, (b) anomalous hall effect (AHE), (c) spin hall effect (SHE), (d) quantum hall effect (QHE), (e) quantum anomalous hall effect (QAHE), (f) quantum spin hall effect (QSHE).	2
1.2	The figure illustrates geometrical objects categorized by their genus, which is a topological invariant representing the number of “holes” or handles in a surface. From left to right: a sphere (genus 0) has no hole, a torus (genus 1) has one hole, the double torus (genus 2) has two holes, and a higher-order surface (genus 3) has three holes.	4
1.3	The figure illustrates the classification of topological materials. TMs are broadly categorized into topological insulators, topological crystalline insulators, and topological semimetals. TSMS further include Dirac semimetals, Weyl semimetals, and nodal-line semimetals, by their band-crossing features in momentum space.	5
1.4	The figure shows how edge states can appear at the interface of a topological insulator wedged between two trivial insulators. The varying topology in the middle results in "band inversions". Bands of equal parity (shown in purple/green here) need to be linked throughout the sample, which results in the emergence of conduction channels at the interfaces (in red).	6
1.5	Schematic diagram of Weyl semimetals, Dirac semimetals and drumhead state in nodal-line semimetals.	8

2.1	Schematic representation of the DFT based workflow for topological phases in YP.	16
3.1	The conventional unit cells of the YP in (a) the <i>NaCl-type</i> and (b) the <i>CsCl-type</i> .	19
3.2	The variation in the (a) enthalpies and (b) relative volume as a function of hydrostatic pressure for the <i>NaCl-</i> and the <i>CsCl-type</i> structures. The structural phase transition pressure is marked with the arrow. The phonon band structures of YP at (c) ambient pressure and (d) structural phase transition pressure.	20
3.3	The variation of the (a) elastic constants and (b) elastic modulus with applied hydrostatic pressure.	21
3.4	The projected density of states (PDOS) of the YP using (a) GGA-PBE+SOC and (b) HSE06+SOC functionals. The projected bulk band structure of this material using (c, d) GGA-PBE and (e, f) HSE06 functionals, without and with SOC, respectively. (g) The Surface Density of State (SDOS) and (h) the Fermi arc at arc energy 0.00 eV along the (001) plane.	23
3.5	The projected bulk band structure of the material YP (a) without and (b) with SOC at 26.5 GPa hydrostatic pressure. (c) The Surface Density of State (SDOS) is plotted along the (001) plane, where the Dirac cone can be seen and relatively flat surface states (inset). Fermi arc at arc energy (d) 0.00 eV and (e) -0.40 eV along the (001) plane.	24
3.6	The evolution of the Wannier charge centers (WCCs) at (a) ambient pressure and (b) 26.5 GPa pressure. (c) A change of the first \mathbb{Z}_2 topological invariant (ν_0) in response to rising the hydrostatic pressure.	27

LIST OF SYMBOLS AND ABBREVIATIONS

Acronym/Symbol	Full Form
TPT	Topological phase transition
Tis	Topological insulators
RE-M	Rare-earth monpnictides
YP	Yttrium phosphide
DFT	Density functional theory
HSE06	Heyd-Scuderia-Ernzerhof
LDA	Local density approximations
GGA	Generalized gradient approximations
PBE	Perdew-Burke-Ernzerhof
BTE	Boltzmann transport equations
DOS	Density of States
SDOS	Surface Density of States
PDOS	Projected Density of States
TSSs	Topological surface states
Å	Angstrom
eV	Electron-volt
TRS	Time-reversal symmetry
2D	Two-dimension
3D	Three-dimensional
TCIs	Topological crystalline insulators
TSMs	Topological semimetals

ARPES	Angle-resolved photoemission spectroscopy
DSMs	Dirac semimetals
WSMs	Weyl semimetals
NLSMs	Nodal line semimetals
TPSMs	Triply degenerate band crossings
MLWFs	Maximally localized Wannier functions
WCCs	Wannier charge centers
IS	Inversion symmetry
BZ	Brillion zone
SPT	Structural phase transition
PAW	Projected augmented wave
B	Bulk modulus
E	Young's modulus
G	Shear modulus
TB	Tight-binding
TRIM	Time-reversal invariant momenta

Topology has emerged as a unifying paradigm in condensed matter physics, providing a deep tool for the understanding and classification of quantum phases of matter. Starting from the original ideas brought forth by the Hall Effect and its quantum analogue, the discipline has broadened to encompass topologically nontrivial phases such as the quantum spin Hall effect, topological insulators, and topological semimetals in general. Such phases are not defined by traditional mechanisms of symmetry breaking but by global topological invariants that control topologically robust surface and edge states. Of interest are \mathbb{Z}_2 topological semimetals, which sit at the phase boundary between topological insulators and trivial metals with gapless bulk states yet still possessing nontrivial topological characteristics. These developments have profoundly redefined the science of electronic materials and hold out promising opportunities for future applications in spintronics and quantum computing.

The journey began with the discovery of the Hall effect by Edwin Hall in 1879 [1], which demonstrated the development of a transverse voltage in a conductor subjected to a magnetic field. This phenomenon laid the groundwork for understanding charge transport in materials. The field advanced significantly with the discovery of the quantum Hall effect (QHE) in 1980 by Klaus Von Klitzing, who observed that the Hall conductance becomes quantized under low temperatures and strong magnetic fields [2]. This quantization was later understood to be governed by topological invariants, specifically Chern numbers, linking the conductance to the system's topological properties [3]. Subsequent developments introduced the quantum spin Hall (QSH) effect, where spin-polarized edge states are protected by time-reversal symmetry (TRS) even without external magnetic fields [4]. This broadened the topological characterization of materials and culminated in the discovery of new states like topological insulators (TIs) [5–8], topological crystalline insulators (TCIs) [7], and all sorts of topological semimetals (TSMs) [9–12], such as Dirac semimetals (DSMs) [12], Weyl semimetals (WSMs) [11], and nodal-line semimetals (NLSMs) [13–15]. Of specific concern are \mathbb{Z}_2 topological semimetals, which sit at the borderline between topological insulators and conventional metals. These materials have gapless bulk phases with the retention of nontrivial topological properties [9,16]. Collectively, these findings greatly improved the landscape of quantum materials and

have paved the way to future technologies for spintronics and quantum information science [17].

1.1.Hall effect

One of the most important achievements of condensed matter physics in the last thirty years has been the establishment of topology as a central framework for describing quantum phases of matter. The voyage started in 1879, when Edwin Hall worked with thin metallic conductors. He noticed that if an electric current was transmitted through a conductor placed in a perpendicular magnetic field, a voltage arose across its sides [1]. This effect, subsequently given the name of the Hall Effect, was more than a novelty; it was the first experimental window into the behaviour of charge carriers within a material. Measuring this transverse voltage, it was then possible to calculate the sign and density of the carriers, exposing the profound interaction between electromagnetism and material internal structure. Throughout the decades, the Hall Effect was an effective diagnostic instrument, employed extensively in research as well as in technology.

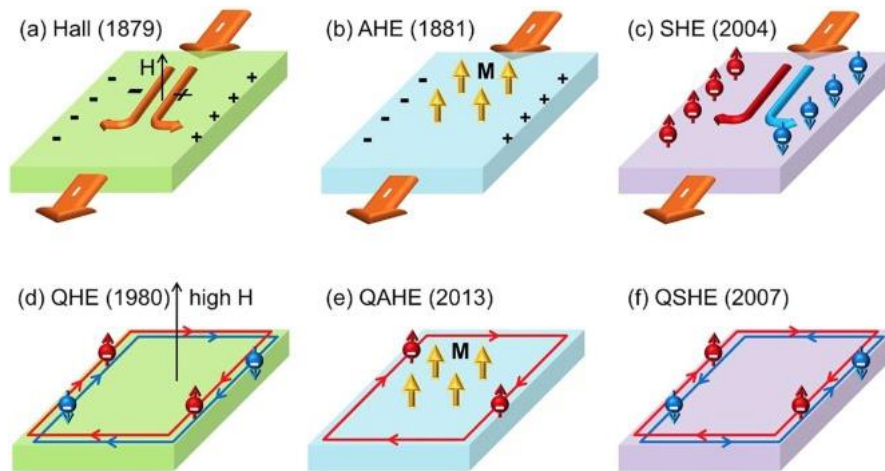


Fig. 1.1 Illustration of Hall effects, (a) conventional Hall effect, (b) anomalous Hall effect (AHE), (c) spin Hall effect (SHE), (d) quantum Hall effect (QHE), (e) quantum anomalous Hall effect (QAHE), (f) quantum spin Hall effect (QSHE) [87].

And then, in 1980, a stunning breakthrough would lift this venerable effect to the quantum world. Klaus Von Klitzing, during experiments with two-dimensional electron gases at extremely low temperatures and powerful magnetic fields, saw something deeply unexpected: the Hall resistance [2] was no longer a smooth, continuous function but rather had quantized

plateaus. The Hall conductance emerged in exact, integer multiples of e^2/h , where e is the elementary charge and h is Planck's constant. This was not merely a precision tool; it was a window into a new type of order in matter, one not controlled by symmetry-breaking but by topology. In contrast to traditional phases of matter based on local order parameters, the Quantum Hall State was described in terms of a topological invariant, an integer called the Chern number [3]. The topological properties led to edge states that were extremely robust, scattering-free from impurities or disorder, ushering in a new paradigm for understanding electronic systems. Still, the QHE needed to be accompanied by strong magnetic fields and ultra-low temperatures, confining its uses. This set physicists wondering whether analogous phenomena were possible under easier conditions. Their answer came with the Spin Hall Effect (SHE), hypothesized theoretically and shortly thereafter evidenced experimentally around the early 2000s [18]. Unlike its predecessors, the SHE did not depend on applied magnetic fields. Rather, it was a consequence of the spin-orbit coupling inherent in some materials, a relativistic interaction between an electron's spin and its motion within the crystal lattice. In this effect, when current is passed through a material, electrons with opposite spins are deflected in opposite directions, piling up at the transverse edges of the sample. Consequently, a clean spin current travels without a concomitant charge current. This spin accumulation at the interfaces suggested the potential for dissipationless spin transport, an idea that would form the core of the field of spintronics [19].

The discovery that topology might control the spin's behaviour even when there were no magnetic fields involved was a deep paradigm shift in our understanding of quantum systems. This started as a classical phenomenon of charge deflection but had now matured into a story where the connectivity and geometry of quantum states, not local symmetries by themselves, controlled the intrinsic properties of materials. This change of outlook predicted that some electronic phases could be stabilized not by energy gaps but by more profound mathematical principles based on topology. These new ideas hinted at the potential for the existence of totally new states of matter, where stable edge or surface phenomena would emerge naturally from the material's quantum wavefunction structure. These systems, resilient to local disturbance and randomness, held out the promise of overturning and reordering the classical solidifications, leading to one of the most thrilling pages of condensed matter physics [20].

1.2. Topology

Topology is a branch of mathematics concerned with the intrinsic properties of space that do not change under continuous stretches, bends, or compressions, provided they are not torn or glued. One way to type topological objects is by an integer called the genus (g), which is the number of holes or handles in a surface. For example, a sphere is of genus 0, and a torus (doughnut) is of genus 1 [21]. Such a system has given rise to the discovery of a new class of materials known today as topological materials. These systems possess non-trivial topological order in their bulk band structure, which leads to conducting states at their surfaces or edges, even though they are insulators or semimetals in the bulk [3]. The presence of such boundary states is not accidental but is assured by the topological character of the bulk and is frequently stabilized by intrinsic symmetries like time-reversal, particle-hole, or crystalline symmetry [8]. Importantly, these surface or edge states have robustness to moderate disorder, impurities, and other perturbations and are hence both fundamentally interesting and technologically attractive.

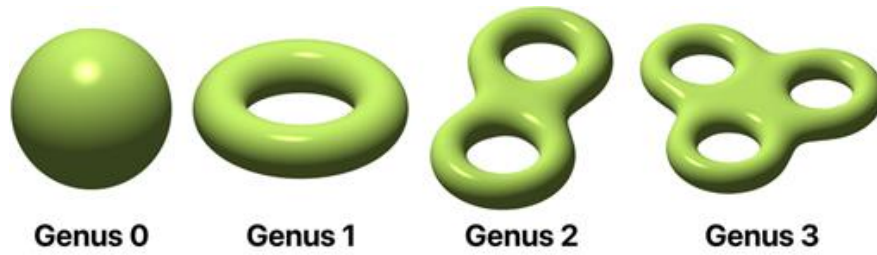


Fig. 1.2 The figure illustrates geometrical objects categorized by their genus, which is a topological invariant representing the number of “holes” or handles in a surface. From left to right: a sphere (genus 0) has no hole, a torus (genus 1) has one hole, the double torus (genus 2) has two holes, and a higher-order surface (genus 3) has three holes [88].

Topological materials (TMs) may further be divided on the basis of the type of their topological invariants and the protecting symmetries of their surface states. The most established category is that of TIs, whose defining characteristic is a bulk band gap with metallic surface states that are protected by TRS [4,3]. A closely associated class is that of TCIs, where the surface state protection comes from crystalline symmetries like mirror, rotational, or glide symmetries [22]. Another important class includes the TSMs, which include DSMs, WSMs and NLSMs. [11-15]. In such materials, the conduction and valence bands cross at sharp points or lines of momentum space to form relativistic quasiparticles and host a variety of exotic transport properties. In addition to these, the subject still advances with new discoveries of phases in the

forms of topological superconductors, higher-order topological insulators, and symmetry-enriched topological phases, evidencing the versatility and richness of topology as an intellectual paradigm of present-day materials physics [23].

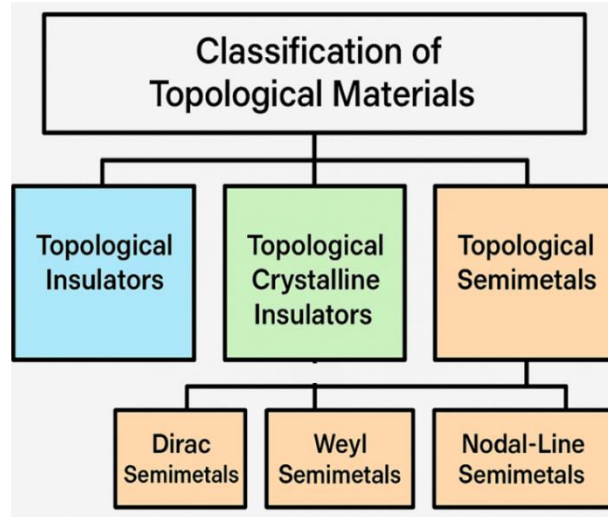


Fig. 1.3 The figure illustrates the classification of topological materials. TMs are broadly categorized into topological insulators, topological crystalline insulators, and topological semimetals. TSMs further include Dirac semimetals, Weyl semimetals, and nodal-line semimetals, distinguished by their band-crossing features in momentum space.

1.3. Topological Insulators (TIs)

The realization of TIs has been one of the greatest advancements in condensed matter physics in the 21st century. TIs challenge traditional classification by displaying insulating behaviour within the bulk yet possessing stable, conducting states along their edges [5] at the same time. This seemingly paradoxical combination of insulating and metallic behaviour comes not from symmetry breaking or local order parameters but rather from the topological nature of the electronic band states in the momentum space. TIs represent a new kind of quantum matter, wherein topological invariants protected by symmetries like TRS led to physical observables that are robust against local perturbations [8]. The theoretical basis of topological insulators lies in the QHE, where the conductance is quantized and is determined by an integer-valued topological invariant, which is called the Chern number. The QHE, however, necessitates strong magnetic fields that destroy TRS, restricting its technological applications. The theoretical problem, therefore, was to find a system where topologically protected conducting states might be present without the necessity of an external magnetic field. This prompted the

groundbreaking research of Kane and Mele in 2005, who put forward a theoretical model based on graphene with spin-orbit coupling. Their theory predicted a new phase of matter, the quantum spin Hall insulator, defined by TRS-protected edge states instead of a magnetic field, and by a new topological invariant: the Z_2 index [1]. This prediction formed the basis of the experimental realization of two-dimensional (2D) topological insulators. Bernevig, Hughes, and Zhang in 2006 suggested that HgTe/CdTe quantum wells are capable of achieving such a phase when the thickness of the HgTe is above a certain critical value and results in band inversion induced by strong spin-orbit interaction [24]. This prediction was experimentally verified in 2007 by König et al., who measured quantized edge conductance characteristic of topologically protected edge states [25]. The 1D edge channels show spin-momentum locking, in which electrons with opposite spins travel in opposite directions, resulting in helical edge modes. Backscattering is forbidden by TRS in the absence of magnetic impurities, leading to dissipationless edge transport.

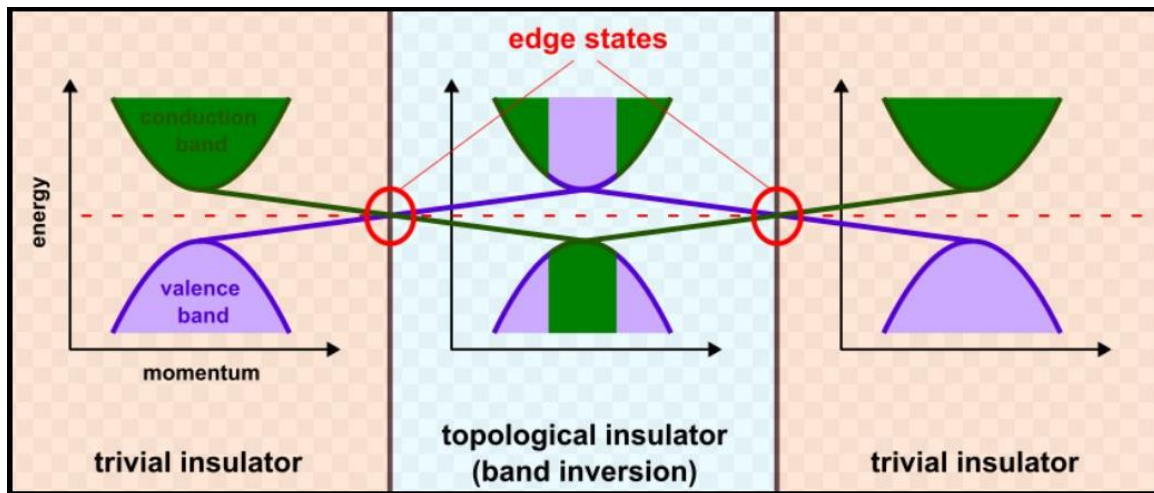


Fig. 1.4 The figure shows how edge states can appear at the interface of a topological insulator wedged between two trivial insulators. The varying topology in the middle results in "band inversions". Bands of equal parity (shown in purple/green here) need to be linked throughout the sample, which results in the emergence of conduction channels at the interfaces (in red) [89].

Following the success with two dimensions, the theory for three-dimensional (3D) topological insulators was introduced shortly after that. Fu, Kane, and Mele developed the Z_2 topological class in three dimensions in 2007, identifying a new topological invariant capable of describing strong and weak topological phases for bulk materials [26]. The signature of a good 3D

topological insulator is the occurrence of gapless Dirac-like surface states that emerge at the surface between the TM and a trivial insulator or vacuum. Such surface states are an odd number of Dirac cones that are protected against localization and scattering by TRS. Experimental synthesis of 3D TIs came in 2008–2009 by discovering topological surface states (TSS) of TCI nature in Bi-based compounds, like Bi_2Se_3 [27], Bi_2Te_3 [28] and Sb_2Te_3 [29]. A single Dirac cone in the surface electronic spectrum made them perfect for testing topological effects. The appearance of such Dirac-like surface states has been visualized successfully by means of angle-resolved photoemission spectroscopy (ARPES) [30] with unbelievable accuracy, reinforcing theoretical predictions to an amazing precision. Theoretical and experimental advances in 2D and 3D TIs have dramatically increased the terrain of quantum phases. Topology in 2D topological insulators, for example, quantum spin Hall systems, guarantees edge modes in one dimension. These edge states may carry non-dissipative spin currents with good implications for low-power spintronics devices. Conversely, 3D TIs host 2D surface states with linear dispersion and spin-momentum locking that can be potentially controlled by magnetism, superconductivity, or an external field.

1.4. Topological Semimetals (TSMs)

The discovery that the insulators have been classified as ordinary insulators and TIs has prompted analog classifications in the metals. Eventually, it came to be understood that the metals can also be classified as ordinary metals and topological semimetals TSMs. In the TSMs, the bulk energy bands cross each other, and there is an emergence of gapless electronic states in the bulk. These gapless properties are frequently secured by some symmetries, including crystal symmetries, TRS, or spatial inversion symmetry [31]. TSMs are further categorized into different types, such as DSMs, WSMs and NLSMs, as shown in Figure 1.5.

1.4.1. Dirac Semimetals (DSMs)

In DSMs, the conduction and valence bands cross over each other at discrete points in the Brillouin zone, referred to as Dirac points, that are four-fold degenerate. The electronic states near these points obey the Dirac equation, and the energy bands exhibit a linear dispersion in every direction of momentum [32]. Due to this Dirac-like character, DSMs show a variety of interesting physical properties, such as very high carrier mobility, high magnetoresistance, high carrier density, and very good electrical conductivity [33].

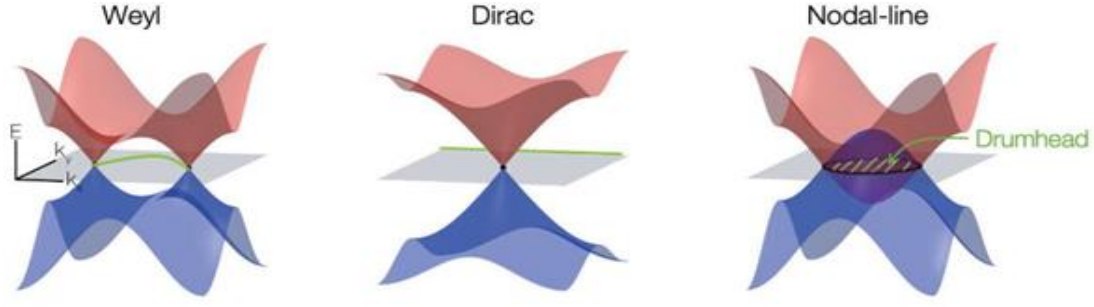


Fig. 1.5 Schematic diagram of Weyl semimetals, Dirac semimetals and drumhead state in Nodal-line semimetals [90].

1.4.2. Weyl semimetals (WSMs)

From the DSMs by breaking TRS or inversion symmetry, condensed matter physics gets WSMs. Dirac points in DSMs are fourfold degenerate. When one of these symmetries is violated, every Dirac point splits into a pair of twofold-degenerate Weyl points with opposite chirality. In addition to these bulk Weyl points, WSMs have characteristic surface states known as Fermi arcs. These arcs start at the surface projections of Weyl points and are used to join Weyl nodes of opposite chirality. The Weyl nodes and Fermi arcs together constitute the most important signatures of WSM [34].

1.4.3. Nodal-Line Semimetals (NLSMs)

The concept of NLSMs was originally proposed by Burkov and co-workers in 2011. In contrast to Weyl or Dirac semimetals, where band crossings are at discrete points, NLSMs have band degeneracies that lie along one-dimensional lines in the Brillouin zone [35]. These novel band structures constitute a new class of materials. Over the last few years, topological semimetals have been a central concern in condensed matter physics. Progress on various fronts has been achieved, such as theoretical modelling, novel material synthesis, and exact experimental studies. This work has unveiled many materials with topologically nontrivial electronic bands and the observation of interesting physical effects. This fast-developing branch shows promise for future technology, especially in spintronics and optoelectronics, where TSM might become a game-changing factor [36].

1.4.4. Z_2 Topological Semimetals

A more subtle and refined class of materials appeared: the Z_2 TSM. They were not trivial metals or complete topological insulators. Rather, they occupied the phase boundary in between, a precarious critical regime where the bulk bands had inverted, as in a topological insulator, but hadn't developed a full energy gap [37]. Interestingly, in spite of this gapless spectrum, the system still had a non-trivial Z_2 index, and with it, most of the surface phenomena characteristic of topological order [38]. The simplest way to appreciate their uniqueness is by contrast. In traditional semimetals like bismuth, the limited overlap between the conduction and valence bands is not protected by symmetry or topological charge; any small perturbation could move or annihilate the band contact [39]. In Dirac and Weyl semimetals, crossings are stabilized by symmetry and topological charge, but at the price of broken TRS or inversion symmetry [13]. Topological insulators, on the other hand, are fully insulating in the bulk but with conducting surfaces ensured by topology. But the Z_2 TSM occupy a niche of their own, materials with a metallic bulk, topology intact, and surface possibly still harbouring robust states, especially on some crystal faces [40]. This state typically occurs at the tipping point of a topological phase transition. Imagine a material such as $ZrTe_5$ [41] or $HfTe_5$ [42], which can be pushed from a robust topological insulator to a weak topological insulator, or even to a trivial metal, merely by adjusting the temperature, pressure, or chemical surroundings [43]. Here at this crucial juncture, when the band gap closes but not the band inversion, the material enters the arena of the Z_2 TSM [44]. It is here that the topology and the metallicity harmonize, not in opposition to each other, but in an exquisitely fine symphony. The fingerprints of such materials are subtle but unambiguous. Their bulk electronic structure exhibits band inversion, the characteristic signature of topological order, and the points at which the bands meet are not to be easily eliminated unless one shatters critical symmetries such as time-reversal or particular crystal symmetries [45]. Although there is no full band gap, the surface can still support Dirac-like states that are similar to a three-dimensional topological insulator. These can be detected using advanced tools like ARPES, where the spin-momentum locking of surface electrons becomes a vivid experimental signature [46]. But most compelling of all is the tunability of Z_2 TSM. Because they exist so precariously at the border between phases, tiny perturbations (a modification in lattice constant, a pressure shift, or even a thermal gradient) can tip them toward a gapped insulating phase or toward a more metallic regime [43,47]. This makes them perfect labs to probe quantum criticality, where the very character of electronic phases changes under ongoing transformation.

1.5. Objective

This thesis is aimed at contributing to the ongoing search and characterization of novel quantum materials exhibiting non-trivial topological phases. With this motivation, the study is structured around the following core objectives:

- To optimize the crystal structure and calculate the structural phase transition in the rare-earth material yttrium phosphide.
- To analyze the mechanical and dynamical stability of the yttrium phosphide compound under ambient and applied hydrostatic pressure.
- To investigate the electronic structure at ambient pressure and obtain the topological phase transition with applied hydrostatic pressure.
- To examine the topological properties, i.e., band inversion, surface state and Fermi arc at ambient and applied hydrostatic pressure.
- To calculate the Z_2 topological invariants using parity analysis and evolution of Wannier charge centers (WCCs).

1.6. Summary

Topology has revolutionized condensed matter physics by unveiling new means for categorizing quantum materials according to global properties of their electronic band structures. With the QHE, there was quantized conductance and topological invariants. Later, the community broadened into topological insulators, those with insulating bulk and surface-conducting, symmetry-protected states. Subsequent discoveries gave rise to topological semimetals such as DSM, WSM and NLSM, in which band crossings in the bulk result in exotic surface states such as Fermi arcs. There is a newer class, Z_2 TSM, which occurs at critical points between topological and trivial phases, with tuneable properties and rich potential for quantum technologies.

CHAPTER 2

METHODOLOGY

Topological properties were studied through first-principles calculations within the density functional theory. Structure and mechanical stability analyses were carried out with VASP based on the PAW method and the GGA for exchange-correlation effects. Electronic structures were checked with spin-orbit coupling to uncover potential topological features. Symmetry analysis was employed to determine band degeneracies associated with the non-trivial topology. The Topological invariants were calculated via Wannier charge center evolution by employing Wannier90 and WannierTools. The surface state calculations also verified the topological phase of the material. This integrated computational approach delivers a comprehensive description of the electronic and topological behaviour of the system.

2.1. Introduction

The study of topological properties was carried out using density functional theory-based first-principles calculations. The simulations were performed using Vienna Ab Initio Simulation Package (VASP) with the projector augmented wave method and generalized gradient approximation for exchange-correlation effects [48]. Structural optimization was followed by analysis of mechanical stability through the calculation of elastic constants. Electronic properties were studied by calculating band structures and density of states. To examine topological characteristics, spin-orbit coupling (SOC) was included in band structure calculations. Symmetry analysis was performed to understand the role of crystal symmetry in band degeneracy and topological behavior. Topological invariants were determined by evaluating the evolution of Wannier charge centers using Wannier90 and the Wannier tool [49,50]. Surface state calculations were also performed to confirm the non-trivial topological phase. All computational tools employed in this study include VASP, Wannier90 and Wannier tool. In the following sections, the computational methods and packages are discussed in detail.

2.2. Density Functional Theory (DFT)

The density functional based method is one of the most popular theoretical methods for electronic properties of materials at the atomic level. It is the backbone of contemporary computational condensed matter physics and material science. The approach is based on the principle that ground-state properties of an interacting many-electron system can be fully

specified by its electron density, as opposed to the complicated many-body wave function. The basic thought behind this method is the mapping of a complicated many-body problem into an easier one by taking recourse to a system of non-interacting electrons that have the same electron density as the interacting system in question. This mapping considerably eases the computational complexity at the expense of none of the important physics. This theoretical concept became feasible with the advent of the Kohn-Sham (KS) formulation, which gives a means to solve for the ground-state electron density through the use of self-consistent field methods. The KS equations are a collection of single-particle equations that are simpler to solve numerically. The validity of this approach is highly dependent on the proper modelling of the exchange-correlation energy, a phrase that describes the quantum mechanical interactions between electrons, such as their mutual repulsion and quantum exchange effects. In the KS version of DFT, the many-electron problem of interacting electrons is solved by a set of non-interacting electrons defined in terms of the following self-consistent equations:

$$\left[-\frac{\hbar^2}{2m} \nabla^2 + V_{eff}(r) \right] \Psi_i(r) = \epsilon_i \Psi_i(r) \quad (2.1)$$

Here $\Psi_i(r)$ are the KS orbitals, ϵ_i are the associated eigenvalues and $V_{eff}(r)$ is the effective potential, given by:

$$V_{eff}(r) = V_{ext}(r) + V_H(r) + V_{XC}(r) \quad (2.2)$$

Here $V_{ext}(r)$ is external potential, $V_H(r)$ is the Hartree Potential and $V_{XC}(r)$ is the exchange correlation potential. The electron density is derived from the Kohn-Sham orbitals as:

$$n(r) = \sum_i^{occ} |\Psi_i(r)|^2 \quad (2.3)$$

These equations are then solved iteratively until self-consistency is established that is, until input and output electron densities agree. Over the last few decades, the density functional based method has been extremely successful in the prediction of a broad spectrum of material properties such as structural stability, electronic band structure, magnetic ordering, and even topological features. It is especially useful for the investigation of new materials like topological insulators, superconductors, and thermoelectric, where experimental information can be scarce or hard to obtain [51].

2.3. Exchange-Correlation Functionals

The exchange-correlation functional is the key ingredient in DFT. It embodies the combined impact of exchange and correlation electron interactions that are two quantum mechanical effects that are difficult to represent accurately. As the precise form of this functional is not known for the majority of real systems, several approximations have been formulated to render DFT computationally useful. The way the electron density and its spatial fluctuation are treated in these approximations varies, leading to a range of functionals with different strengths and limits. The Local Density Approximation (LDA), Generalized Gradient Approximation (GGA), and Hybrid Functionals are the most commonly utilized forms. Each has particular uses depending on the kind of system being studied.

2.3.1. Generalized Gradient Approximation (GGA)

The GGA is a development beyond LDA in that the electron density at every point and how it varies in space are taken into account. This permits GGA functionals to have a more realistic description of the behaviour of inhomogeneous electron systems, such that they can be more accurately used for molecules, surfaces, and transition metal oxides. GGA fixes many of the deficiencies of LDA, making more accurate predictions of lattice parameters, cohesive energies, and magnetic properties. The most popular GGA functionals are the Perdew-Burke-Ernzerhof functionals [52]. GGA is usually regarded as the norm for most solid-state DFT calculations because it provides a good balance between accuracy and computational expense.

2.3.1.1. Perdew–Burke–Ernzerhof (PBE)

The PBE functional is among the most popular GGA functionals. It is an improvement over the LDA since it includes the gradient of the electron density, enabling it to better handle inhomogeneities. In this study, PBE was selected for the exchange-correlation potential because of its compromise between computational cost and structural and electronic property reproduction accuracy. PBE is particularly accurate for the study of semiconductors and transition metal compounds, and is used in most conventional DFT codes, such as VASP [48].

2.3.2. Hybrid Functionals

Hybrid functionals provide even higher accuracy by adding a portion of the exact exchange

energy computed from Hartree-Fock theory to the exchange-correlation functional. This mixing is able to counter some of the built-in shortcomings of fully local or semi-local functionals like LDA and GGA, especially in the description of electronic band gaps. Hybrid functionals are particularly good for systems where electronic correlation is important, i.e., in strongly correlated materials, organic molecules, and wide band gap semiconductors. Some common hybrid functionals are HSE06, which is widely used in solid-state physics [53]. Hybrid functionals are more computationally intensive but provide a much better accuracy in the prediction of electronic structure and optical properties.

2.4. Computational packages

2.4.1. VASP

The VASP is a tool employed for conducting quantum mechanical calculations. This involves the use of PAW, coupled with a plane wave basis set [48]. VASP solves the many-body Schrödinger equation approximately by solving the KS equation (in the framework of DFT) or by solving the Roothaan equations (in the framework of the Hartree-Fock approach). Additionally, certain hybrid functionals that inherit aspects from both the Hartree-Fock approach and the DFT are also available [53]. VASP calculates key quantities through a plane wave basis: single-electron orbitals, charge density, and local potential. The exchange the electrons and ions is either expressed with the help of the PAW method or with the help of norm-conserving or ultrasoft pseudopotentials [48]. VASP carries out calculations using 4 necessary input files, which are

- **INCAR:** This file is used to determine what kind of calculation has to be done on the investigated system. There are certain tags specified in the INCAR file which we have to set to select a certain algorithm and set the parameters.
- **POSCAR:** This file gives the details of the system that we study. it consists of the atomic positions in the unit cell and the translational vectors.
- **POTCAR:** This file consists of the pseudopotential for every single atomic species which is present in Mendelev's.
- **KPOINTS:** This file sets the mapping for the irreducible Brillouin zone in the crystal reciprocal lattice structure.

2.4.2. Wannier90

Wannier90 is an open-source tool designed to construct maximally localized Wannier functions (MLWFs) from DFT outputs [49]. In this study, it played a crucial role in generating a tight-binding Hamiltonian that accurately reproduces the *ab initio* band structure, particularly near the Fermi level. The process started with the `wannier.win` file which defines the projections, number of bands, frozen and disentangled energy windows, and other parameters necessary for Wannierization. The `wannier.eig` file provided the band eigenvalues of VASP, while the `wannier.mmn` and `wannier.amn` files contained matrix elements and projection overlaps, respectively. These were necessary for the localization process and the formation of MLWFs. The output Wannier functions maintained the symmetry and character of the initial atomic orbitals but were spatially localized, which is very important in investigating topological properties.

2.4.3. WannierTools

WannierTools is a versatile software package employed to investigate the topological properties of materials based on tight-binding models extracted from Wannier90 [54]. In this paper, WannierTools was used to compute the evolution of Wannier charge centers (WCCs), which is a stable approach to test the Z_2 topological invariant for time-reversal-invariant insulators. The fundamental input to these calculations is the `wt.in` file that sets a variety of computational parameters such as slab setup, ranges of energy, and surface state analysis paths. Wannier Tools uses iterative Green's functions to calculate surface spectral functions in semi-infinite systems and confirm the existence of topologically stable surface states in the form of Dirac cones or edge modes.

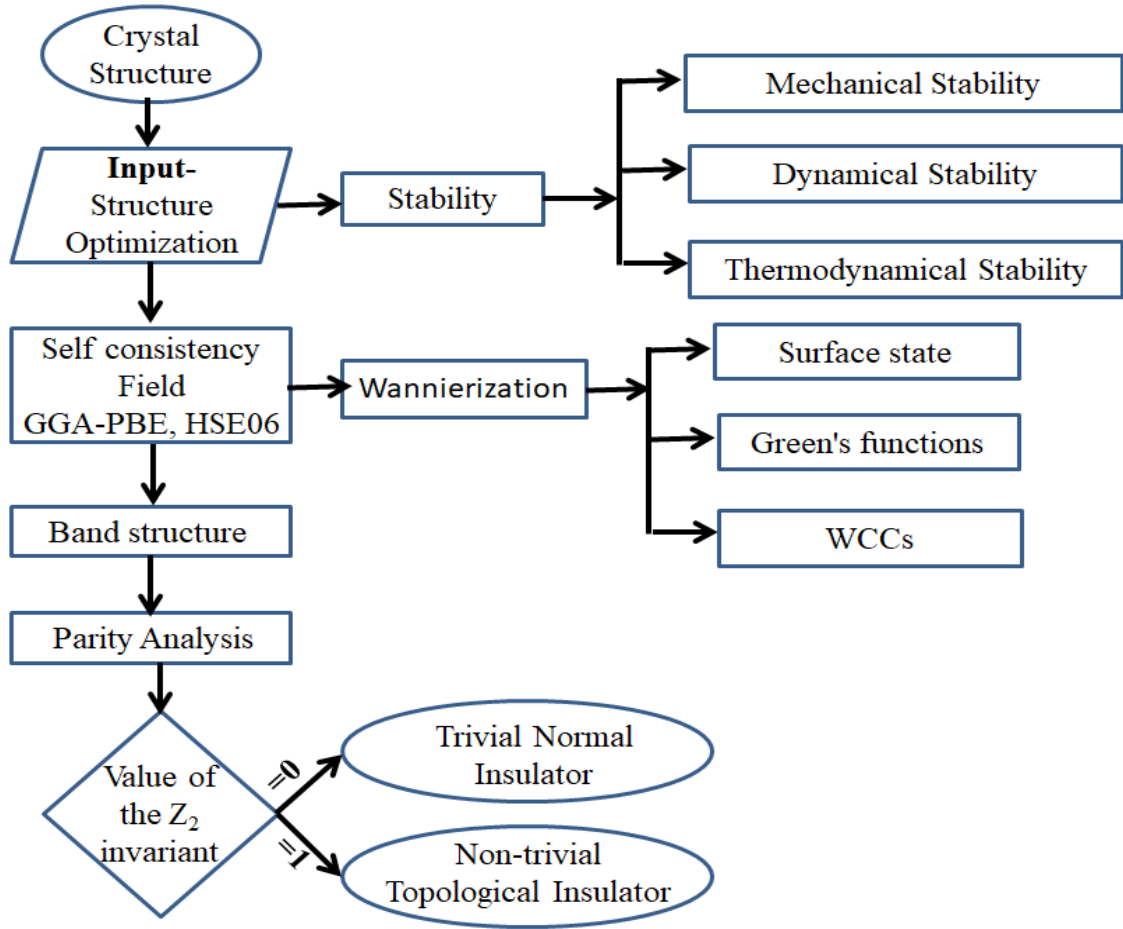


Fig. 2.1 Schematic representation of the DFT-based workflow for topological phases in YP.

2.6. Summary

The study employed DFT using the VASP code with the PAW method and the PBE form of the GGA for exchange-correlation effects. Structural optimization, elastic constants, and electronic properties were evaluated, with SOC included to analyze topological features. Wannier90 was used to generate maximally localized Wannier functions and construct tight-binding models. WannierTools facilitated the computation of Z_2 topological invariants through the evolution of Wannier charge centres and surface state analysis. Hybrid functionals were also discussed for improved band gap accuracy. The methodology integrates electronic structure analysis and topological characterization through VASP, Wannier90, and WannierTools.

CHAPTER 3

STRUCTURAL AND TOPOLOGICAL PHASE TRANSITIONS IN YTTRIUM MONOPHOSPHIDE

Rare-earth mononictides with topological properties have received considerable attention in the condensed matter physics community. Hybrid density functional theory is utilized here to examine the rare-earth semimetal yttrium monophosphide (YP) structural stability, electronic properties, and topological phase transitions subjected to hydrostatic pressure at ambient conditions. YP is found to stabilize in a stable face-centered cubic (NaCl-type) crystal structure at ambient conditions, which persists up to a structural phase transition around 63.6 GPa. Although YP is a topologically trivial semimetal under zero pressure, there is a topological phase transition at approximately 26.5 GPa. The non-trivial topological phase formation is verified through the band inversion around the X-point and the development of a Dirac cone along the (001) surface. In addition, the \mathbb{Z}_2 topological invariants, determined via both the parity analysis at the time-reversal invariant momenta (TRIM) points and the evolution of Wannier charge centers, are equal to (1;000) at 26.5 GPa, confirming the non-trivial topological character of the phase.

3.1. Introduction

The investigation of topological phenomena has emerged as one of the most important areas of research in the field of condensed matter physics in recent years [4, 22, 55]. The TMs have an unusual conducting quantum state at the surface/edge but an insulating nature in bulk [4,55]. These conducting surface states are doubly protected by TRS as well as inversion symmetry (IS) and are robust against impurities and defects [6,7]. SOC plays an important role in TMs [4,22,55]. These materials are identified as topologically non-trivial due to the presence of TSSs and can be characterized by the \mathbb{Z}_2 topological invariant. These TMs can further divide into TIs [6-8], TCIs [7], TSMs [9-12], etc. The TSMs can be categorized into DSMs [12], WSMs [11], and NLSMs [13-15], etc., depending upon the symmetry protection and nature of TSSs. For example, a DSM can be converted into WSM if either TRS or IS is broken [56]. These semimetals have a crossing of the valence band (VB) and the conduction band (CB) at some isolated momenta points in the Brillouin zone (BZ) and a clear gap in eigenstates near the Fermi energy elsewhere. There exist another class of TSMs known as \mathbb{Z}_2 TSM, which have a localized energy band gap in the momentum space and TSS in these materials is protected by

TRS as well as IS [57-58]. The \mathbb{Z}_2 topological semimetals have been realized in rare-earth monopnictides (RE-M); RE: rare-earth elements and M: pnictide elements [59-63]. Several RE-M (RE=Ce, La, Pr, Sm, Gd, Yb; M= Bi, Sb, As, P) have been reported to exhibit topologically semimetallic band structures at ambient pressure [59-63]. The ARPES studies of CeSb and CeBi semimetals [64-65] and *first-principles* investigations of CeSb, CeBi, PrSb, PrBi, SmBi, and GdBi have been reported the topological phases in these materials [60,65-67]. It has been observed that the topological phase transition (TPT) can be induced in RE-M materials via hydrostatic pressure, without disturbing the charge neutrality and the stoichiometry of these materials. The RE-M materials such as LaSb [57], GdSb [68], LaAs [58], TmSb [69], YX (X= As, Sb, Bi) [70,71,72], and YbAs [73] have shown the TPT from trivial to non-trivial topological phase under the applied hydrostatic pressure. The non-magnetic YX (X= N, P, As, Sb, Bi) materials also belong to the RE-M family and their structural stability has been reported over a large range of hydrostatic pressure [75-78]. These materials are semimetallic, and it has been shown that the YAs, YSb and YBi exhibit TPT under hydrostatic pressure and epitaxial strain [70,71,72]. Another member of this family, *i.e.*, YP, also has a semimetallic nature and structural stability at relatively higher pressure in comparison to other members of this family [74-75].

It has been reported that the rare-earth semimetal family YM (M=N, P, As, Sb, Bi) is stable in rocksalt structure throughout a wide hydrostatic pressure range and also have TPT reported in YBi, YSb and YAs materials [70-72]. YP has a similar cubic structure, but the radius and strength of the SOC of the pnictides increased as we moved from N to Bi. The present study is motivated by the in-line structural behaviour of YP with the other members of this family as well as the recent progress of high-pressure synthesis and topological phase studies in materials [76-79]. We have examined the structural stability, electronic, and topological properties of this material.

3.2. Computational details

We have performed *first-principles* calculations within the DFT [80-82] framework using PAW [82] as implemented in the VASP code [48]. The PAW potentials used for Y and P have nine valence electrons ($5s^1 4p^6 4d^2$) and five valence electrons ($3s^2 3p^3$), respectively. To include the exchange-correlation energy, the Perdew Burke Ernzerhof (PBE) [52] of GGA functional, followed by the hybrid functional (HSE06) [53], was used with the inclusion of SOC in the self-consistent field cycle and post-processing. The plane wave cut-off energy and threshold

energy convergence were set at 340 eV and 10^{-6} eV, respectively, for the basis set. The Monkhorst-type [83] k-mesh sampling of $7 \times 7 \times 7$ was used for the mapping of the BZ. The PHONOPY and VASPKIT codes were used to verify the dynamical and mechanical stabilities, respectively, of the system [84, 85]. The tight-binding (TB) model, as implemented in the Wannier90 [54], was used to calculate the MLWFs. The surface state, WCCs, and Fermi arc were calculated using the Green's function approach as employed in the WannierTool code [50].

3.3. Structural properties

The stable *NaCl*-type ($Fm\bar{3}m$) crystal structure is shown in Figure 1(a), in which Y and P atoms have coordinate positions (0, 0, 0) and (0.5, 0.5, 0.5), respectively. Under the applied hydrostatic pressure, this *NaCl*-type structure shows an SPT in the *CsCl*-type structure, Figure 3.1(b). Figure 3.1(c) illustrates the truncated octahedron BZ of the *NaCl*-type crystal structure of this material. The computed enthalpy for both structures, expressed as $H = E + PV$ (with E representing total energy, V and P denoting volume and pressure, respectively), as a function of the applied hydrostatic pressure, is given in Figure 3.2(a). The rocksalt structure, which has the lowest enthalpy, is more stable at ambient pressure, whereas the enthalpy has shown a gradual increment as we applied the hydrostatic pressure, and the *CsCl*-type structure becomes more stable at SPT pressure (P_T), *i.e.*, 63.6 GPa. A comparative analysis of the optimized lattice parameters and the SPT pressure with previous reports is shown in Table 3.1.

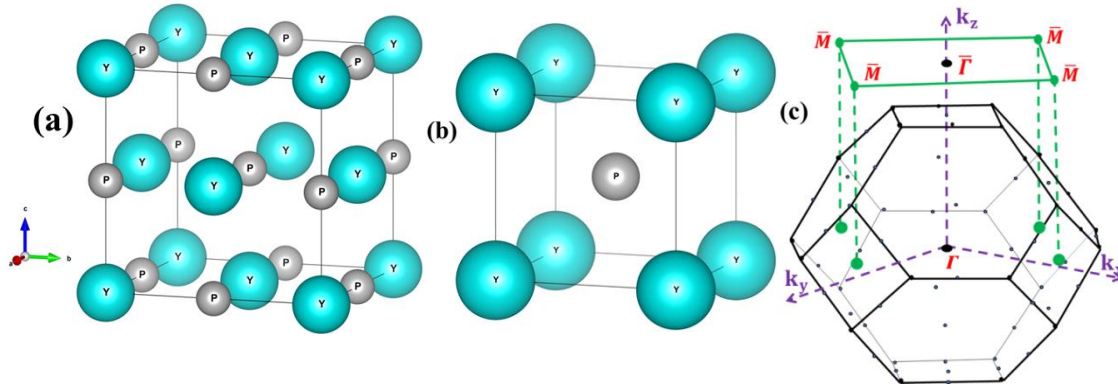


Fig. 3.1 The conventional unit cells of the YP in (a) the *NaCl*-type and (b) the *CsCl*-type crystal structures. (c) The truncated octahedron Brillouin zone (BZ) of YP centered at Γ , with projected (001) plane (green colour) along the k_z -direction.

Table 3.1 The optimized lattice parameter and structural phase transition (SPT) pressure of YP.

YP	Previous studies	Present study
----	------------------	---------------

Lattice parameter, a (Å)	5.6439 [79], 5.683 [75]	5.667
SPT (GPa)	63.8 [79], 55.94 [75]	63.6

3.4. Stability Analysis

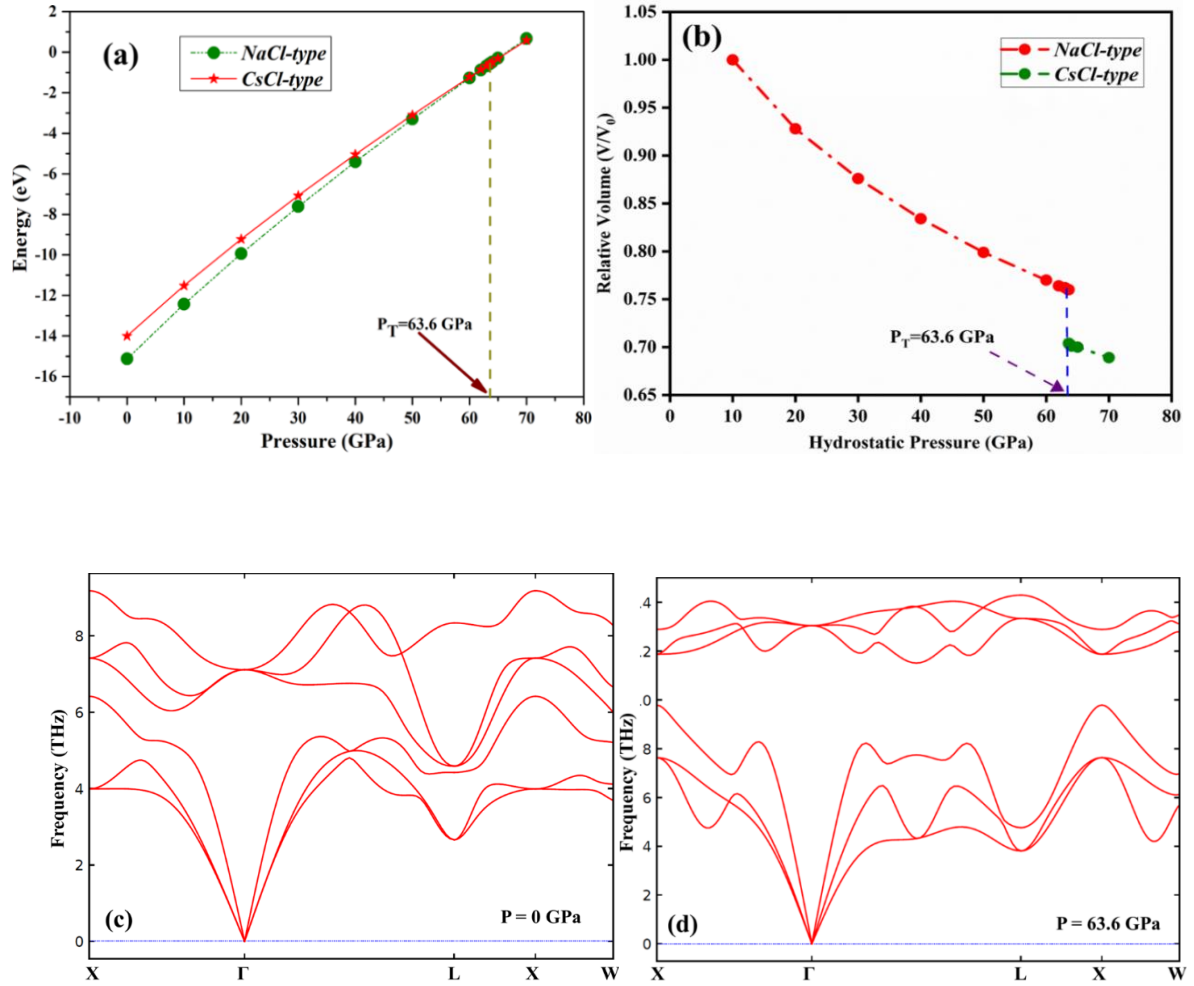


Fig. 3.2 The variation in the (a) enthalpies and (b) relative volume as a function of hydrostatic pressure for the *NaCl*- and the *CsCl*-type structures. The structural phase transition pressure is marked with the arrow. The phonon band structures of YP at (c) ambient pressure and (d) structural phase transition pressure.

The change in relative volume as a function of hydrostatic pressure has shown an abrupt change in relative volume, which confirms the first-order phase transition at the SPT pressure as depicted in Figure 3.2(b). The phonon band structures in Figure 3.2 (c, d) confirm the dynamical stability of the *NaCl*-type structure up to the SPT pressure.

Table 3.2 The values of the various elastic properties at applied hydrostatic pressure.

Hydrostatic Pressure (GPa) Elastic Properties	0	10	20	30	40	50	60	63.6
C_{11}	201.59	294.26	380.6	459.07	530.89	590.76	653.43	677.09
C_{12}	28.57	25.45	24.02	22.28	20.81	20.66	21.69	22.31
C_{44}	47.85	51.96	53.52	55.05	55.79	54.37	53.64	54.95
Bulk Modulus B (GPa)	86.2	115.05	142.88	167.88	190.83	210.69	232.27	240.57
Young's Modulus E (GPa)	147.66	188.65	220.85	249.19	273.25	288.70	305.83	315.58
Shear Modulus G (GPa)	60.79	76.89	88.88	99.47	108.32	113.51	119.42	123.14

We have also analyzed the mechanical stability of YP up to the SPT pressure. For cubic systems, there are three independent elastic constants of the stiffness tensor, i.e., C_{11} , C_{12} , and C_{44} . The Born stability criteria [86] for the mechanical stability of the cubic systems are,

$$C_{11} > 0; C_{44} > 0; C_{11} - C_{12} > 0; C_{11} + 2C_{12} > 0. \quad (3.1)$$

The calculated values of the C_{ij} (Table 3.2) under the various hydrostatic pressures, values have satisfied equation (3.1), which signifies the mechanical stability of this material at ambient and elevated pressure.

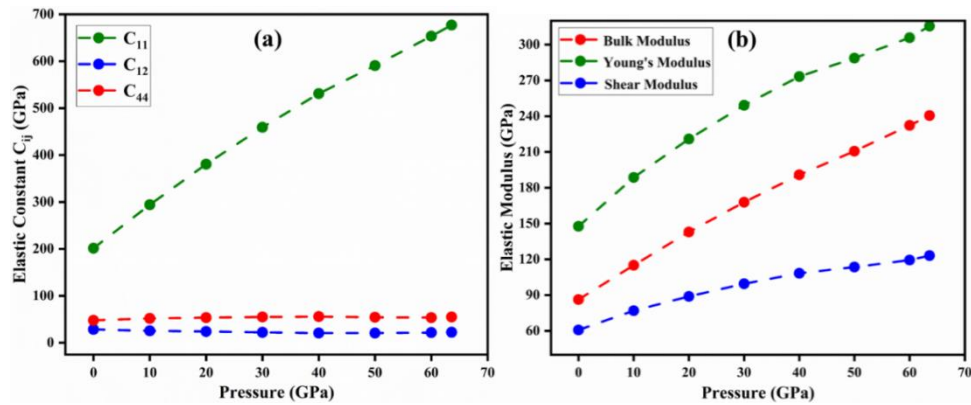


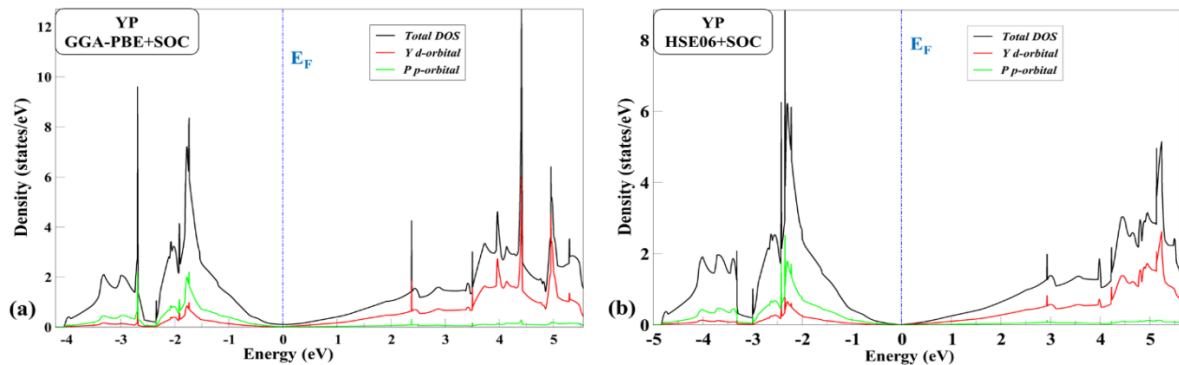
Fig. 3.3 The variation of the (a) elastic constants, and (b) elastic modulus with applied hydrostatic pressure.

Fig. 3.3(a) shows the variation of C_{ij} with the applied hydrostatic pressure, we have observed an increase in C_{11} that suggests the material is stiffer and more resistant to deformation along the a -axis. The other two tensor components, i.e., C_{12} and C_{44} have shown very slow decreases and increases, respectively, which suggests nearly constant shear deformations in the

perpendicular planes. Moreover, the variation of the Bulk Modulus (B), Young's Modulus (E), and Shear Modulus (G) (Figure 3 (b)) has confirmed that the material becomes more incompressible, harder, and resistant towards deformation, respectively, with the increasing applied hydrostatic pressure. Hence, the material exhibits excellent mechanical stability and less susceptibility to deformation at ambient at higher pressure.

3.5. Electronic Structure

To examine the topological phase, we have analyzed the electronic properties of YP using the GGA-PBE+SOC and HSE06+SOC functionals. A slight non-zero density of states (DOS) at the Fermi level (Figure 3.4 (a, b)) and the overlaps between VB and CB at different high symmetry points in the bulk band structure (Figure 3.4 (c-f)) signify that YP is a conventional semimetal. This observation is in good agreement with the previous reports [34-39]. The projected density of states (PDOS) in Figure 3.4 (a, b) and projected band structure shows that the *d-orbital* of Y and *p-orbital* of P are mainly contributing to the VB and CB, respectively, near the Fermi level. The band structures are calculated along the $X-\Gamma-L-X-W$ high symmetry *k-path*, where *X*, Γ , and *L* are the time-reversal invariant momenta (TRIM) points. The value of the energy gap at Γ - and *L-points* evaluated using HSE06 functional (Figure (e, f)) is higher than the GGA-PBE (Figure (c, d)) functional. Moreover, since the former is believed to be more accurate than the latter, we believe that HSE06 functional predicts the accurate ground state of the RE-M materials [76-78]. Therefore, all the further calculations have been performed using this functional only. As depicted in Figure 3.4 (g), the absence of band inversion in the bulk band structure and Dirac cone in the surface density of state (SDOS) along the (001) plane make YP a topologically trivial semimetal at the ambient pressure condition. This nature is further confirmed by the isolated electron and hole pockets at $\bar{\Gamma}$ - and at \bar{M} -points, as visible in Fig. 3.4 (h).



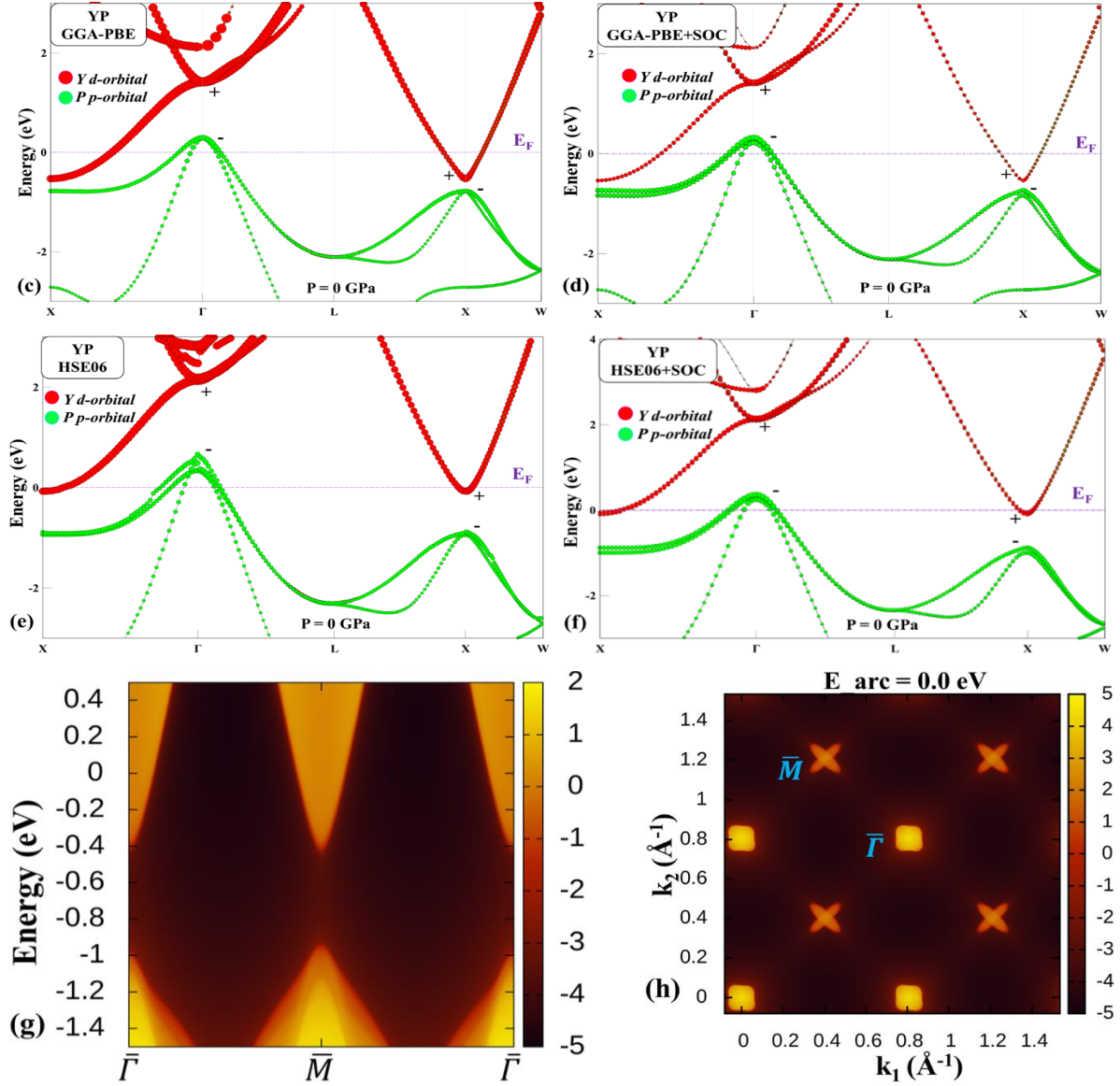


Fig. 3.4 The projected density of states (PDOS) of the YP using (a) GGA-PBE+SOC and (b) HSE06+SOC functionals. The projected bulk band structure of this material using (c, d) GGA-PBE and (e, f) HSE06 functionals, using without and with SOC, respectively. (g) The Surface Density of State (SDOS) and, (h) the Fermi arc at arc energy 0.00 eV along the (001) plane.

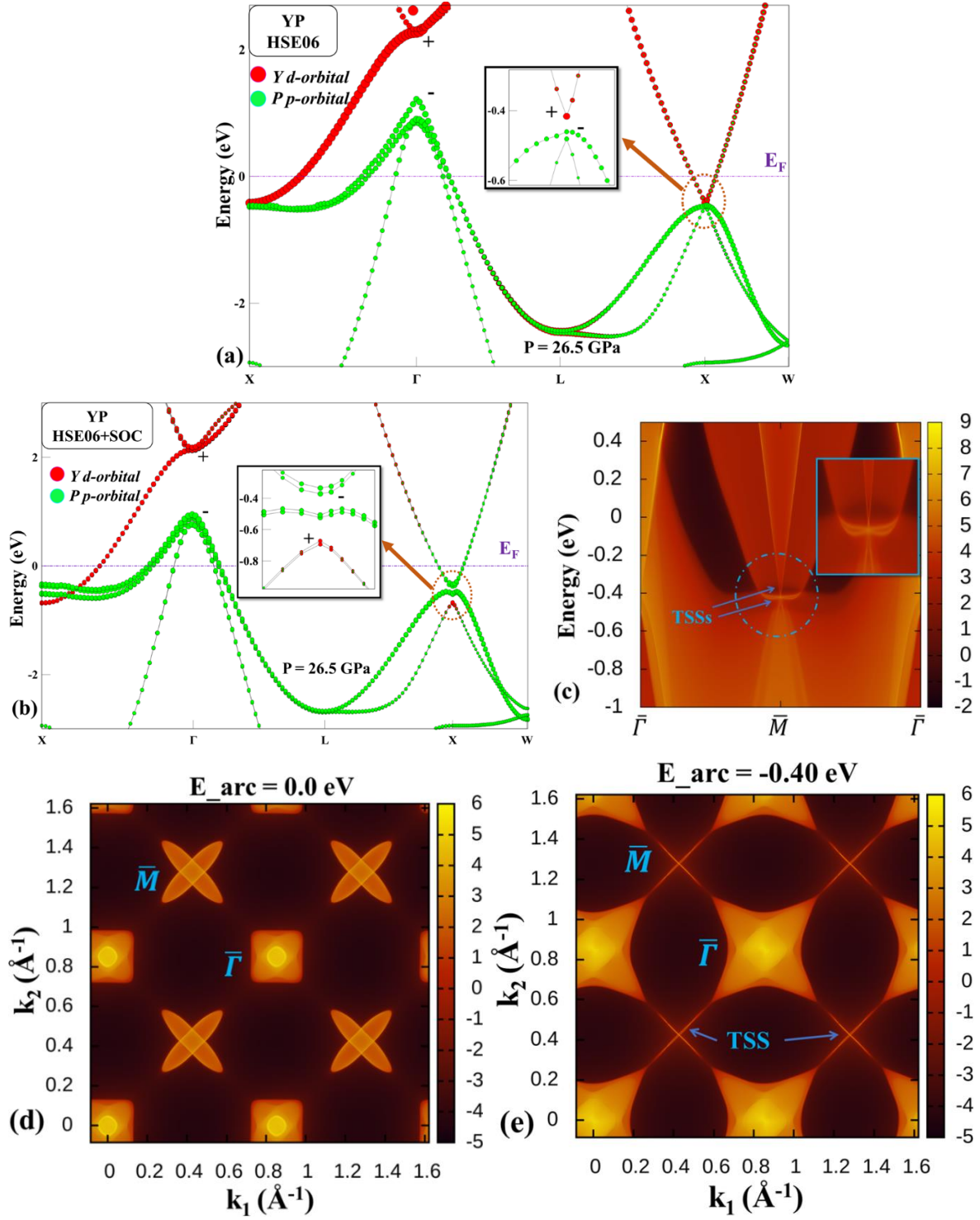


Fig. 3.5 The projected bulk band structure of the material YP (a) without and (b) with SOC at 26.5 GPa hydrostatic pressure. (c) The Surface Density of State (SDOS) is plotted along the (001) plane, where the Dirac cone can be seen and relatively flat surface states (inset). Fermi arc at arc energy (d) 0.00 eV and (e) -0.40 eV along the (001) plane.

To observe the TPT in this semimetal, we continuously increase the pressure up to 26.4 GPa, the energy gap at the Γ - and X -points shows a continuous reduction, but no band inversion is observed till this pressure. At 26.5 GPa, the lattice parameter of the materials has reduced to 5.287 Å and the bulk band structures using HSE06 without and with SOC are shown in Figure 5 (a, b), respectively. A bulk band inversion appears in the band structure at the X -point as shown in Figure 3.5 (b), making YP a topologically non-trivial semimetal. The inverted contribution of the d -orbital of Y in VB and the p -orbital of P in CB is observed at this hydrostatic. This non-trivial phase is further confirmed by the presence of the Dirac cone (Figure 3.5 (c)) at \bar{M} -point along the (001) plane in SDOS at 26.5 GPa. We have observed that the presence of two conducting TSSs at \bar{M} -point is caused by the projection of two inequivalent X -points. A Dirac cone and a relatively flat TSS connected to bulk states have been observed at the \bar{M} -point as shown in the inset of Figure 3.5 (c). The flat TSS lose its conducting nature as it moves away from the \bar{M} -point and disperse into the bulk states having the same orbital character. It is evident from the Fermi surface (Figure 3.5 (d)) at 26.5 GPa pressure that there is one electron pocket and two hole pockets at $\bar{\Gamma}$ -point, which corresponds to the $k_z = 0$ and π , respectively. At TPT pressure, the relative size of the perpendicular electron pockets at the \bar{M} -point is larger than the ambient pressure, and it begins to decrease as Fermi arc energy increases in the negative direction, while the size of the hole pockets at $\bar{\Gamma}$ -point begins to expand. The Dirac cone is visible in SDOS at the Fermi arc energy of about -0.40 eV in the bulk band inversion point (Figure 3.5 (e)), where the spectral contribution from the TSSs at \bar{M} -point can be seen. These TSS have an elliptical shape and a cross-like shape due to a weakly developed continuous link with bulk bands. Additionally, a direct relationship between the TSSs and the bulk states is produced by an increase in pressure. The bulk band inversion is directly demonstrated by the anisotropic dispersion of the TSSs in YP.

3.6. \mathbb{Z}_2 topological invariants

To further verify the appearance of TPT in YP, we have calculated the \mathbb{Z}_2 topological invariant using the product of parities of all the filled bands at the TRIM points. For the bulk material, there are four \mathbb{Z}_2 topological invariants. The \mathbb{Z}_2 topological invariant criteria for TIs can also be implemented on RE-M semimetals due to the presence of a local energy band gap around certain momentum points. There are eight possible TRIM points [5] in the bulk systems, represented by the equation,

$$G_{i=(m_1 m_2 m_3)} = \frac{m_1 a_1 + m_2 a_2 + m_3 a_3}{2} \quad (3.2)$$

Where a_i ($i = 1, 2, 3$) are primitive reciprocal lattice vectors and m_j have values 0 or 1. The adiabatic transformation has changed the sign of parities of the eigenstates in the bulk band structure, and hence the values of the four \mathbb{Z}_2 invariants ($\nu_0; \nu_1 \nu_2 \nu_3$) can be computed using the following equations given by Kane and Mele criteria [4],

$$(-1)^{\nu_0} = \prod_{n_j=0,1} \delta_{n_1 n_2 n_3} \quad (3.3)$$

$$(-1)^{\nu_{i=1,2,3}} = \prod_{n_i=1; n_j=0,1} \delta_{n_1 n_2 n_3} \quad (3.4)$$

Here, δ signifies the product of all the filled bands at a given TRIM point. The value of the first \mathbb{Z}_2 invariant (ν_0) indicates whether the phase of the system is topologically trivial ($\nu_0 = 0$) or non-trivial ($\nu_0 = 1$). The product of parities of the filled bands at different TRIM points at ambient and TPT pressures is depicted in Table 3.3.

Table 3.3 The product of parities of all filled bands at TRIM points in BZ under ambient and exalted pressure values.

Hydrostatic Pressure	No. of band inversions	$3X$	$4L$	Γ	\mathbb{Z}_2 invariants
0 GPa	No inversion	+	+	+	(0:000)
26.5 GPa	One inversion	-	+	+	(1:000)

At the ambient pressure, the product of parities at three X momenta points is positive, whereas a switch from positive to the negative value of parities at these points is observed at 26.5 GPa. With this switch in the parities at three X momenta points, the first \mathbb{Z}_2 topological invariant (ν_0) changes its value from 0 to 1 (Table 3.3). This non-zero value of the first \mathbb{Z}_2 topological invariant has verified the TPT pressure. Moreover, the parties of the three X -points and the four L -points remain positive (Table 3.3) at both ambient and elevated pressure, which concludes that the remaining topological invariants (using equation 3.4) are (000).

Another approach to calculating the \mathbb{Z}_2 topological invariants and identification of the topological phases of materials is the Wilson loop method [49]. In this method, the \mathbb{Z}_2 topological invariants have been computed using the evolution of WCCs along six TRIM planes, *i.e.*, k_j ($j = x, y, z$) = 0, π . The topological state of the material can be established by examining the juncture of Wannier bands with a random reference line along the k_i -axis as shown in Figure 3.6 (a, b).

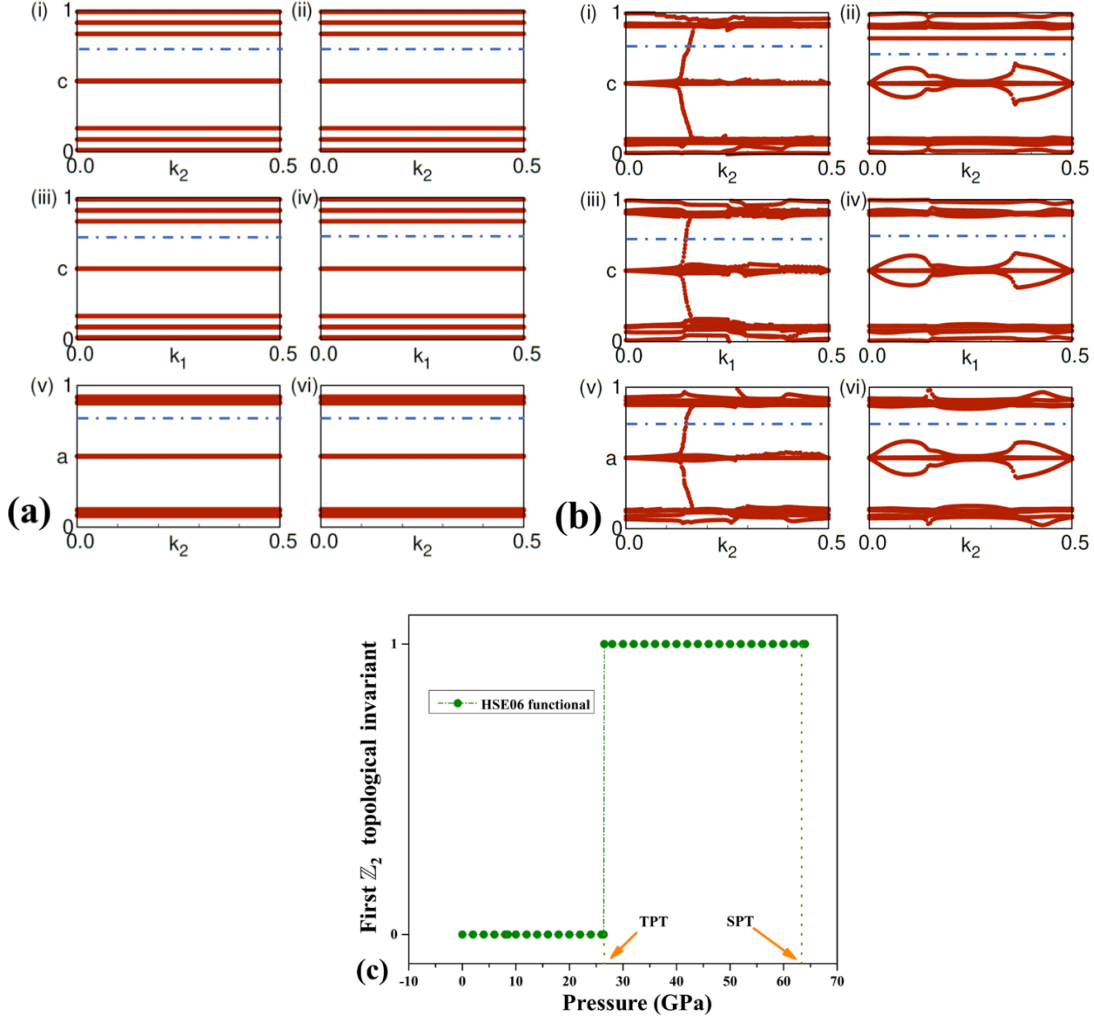


Fig. 3.6 The evolution of the Wannier charge centers (WCCs) at (a) ambient pressure and (b) 26.5 GPa pressure. (c) A change of the first \mathbb{Z}_2 topological invariant (ν_0) in response to rising the hydrostatic pressure.

The number of intersections that occur between the reference line and Wannier bands indicates z_2 value in that TRIM plane and the \mathbb{Z}_2 topological invariants can be calculated as per the following equations,

$$\nu_0 = \{z_2(k_{i=1,2,3}=0) + z_2(k_{i=1,2,3}=0.5)\} \bmod 2 \quad (3.5)$$

$$\nu_{i=1,2,3} = z_2(k_i=0.5) \quad (3.6)$$

According to Figure 3.6 (a), the reference line has not shown any crossing with the Wannier bands in k_j ($j = x, y, z$) = 0, π , and hence the system has a topologically trivial nature with the values of the \mathbb{Z}_2 topological invariants (0; 000). At 26.5 GPa, the reference line and the Wannier

bands have an odd number of crossings along k_j ($j = x, y, z$) = 0 planes but no crossing is observed along k_j ($j = x, y, z$) = π planes as shown in Figure 3.6 (b). Using equations (3.5) and (3.6), the \mathbb{Z}_2 topological invariants can be calculated and have values (1; 000), which has established the topologically non-trivial phase in this material at 26.5 GPa. The observation of bulk band inversion, the presence of the Dirac cone along the (001) plane and the non-zero value of first \mathbb{Z}_2 topological invariant (ν_0), have recognized that the rare-earth semimetal YP have undergone a TPT at 26.5 GPa of hydrostatic pressure. Figure 3.6 (c) illustrates the variation of the first \mathbb{Z}_2 topological invariant (ν_0) with the applied pressure.

3.8. Summary

We have explored the mechanical, structural and dynamical stability, and topological properties of rare-earth semimetal YP using density functional theory and Green's function approach. YP has the *rocksalt-type* stable crystal structure at ambient pressure, and it has been observed that a structural phase transition takes (*CsCl-type* structure) at 63.6 GPa hydrostatic pressure. The dynamical and mechanical stabilities have been verified via the phonon dispersion spectrum and elastic constant calculation, respectively, up to the structural phase transition pressure. This material is topologically trivial at ambient pressure, and its accurate ground state has been predicted with the help of the HSE06 functional. The absence of a Dirac cone in the surface density of state along the (001) plane and (0; 000) values of its four \mathbb{Z}_2 topological invariants at ambient pressure has also been verified as the topologically trivial phase of this material. At 26.5 GPa of applied pressure, a topological phase transition from topologically trivial to non-trivial phase has taken place, and an inverted contribution of the *d-orbital* of Y valence band and *p-orbital* of P has confirmed the topologically non-trivial phase in this material. The presence of a Dirac cone in the surface density of state along the (001) plane has also been observed at 26.5 GPa hydrostatic pressure. The change in the values of the \mathbb{Z}_2 topological invariants to (1; 000) has been calculated using the product of parities and evolution of Wannier charge centers at above mentioned hydrostatic pressure. The comprehensive information from this study could be helpful for future experimental studies of topological states in YP.

CHAPTER 4

CONCLUSION AND FUTURE SCOPE

Based on the detailed analyses and results discussed throughout this thesis, the major conclusions are outlined below, along with prospective future research directions that could further advance the understanding of pressure-tuned topological phases.

4.1. Conclusion

This dissertation investigates the intriguing and quickly developing field of topological quantum materials, particularly their origin based on fundamental physical principles like spin-orbit coupling, band inversion, and protection by symmetry. Starting with the historical establishment of the Hall effects and the paradigm-shifting quantum Hall phenomena, the work slowly introduces the theory of topology in condensed matter systems. Conceptual constructs like the topological invariants of \mathbb{Z}_2 , Dirac and Weyl quasiparticles, and topological surface states are elaborately discussed to establish a firm conceptual background. Topological insulators and semimetals are thoroughly classified with emphasis on their distinct electronic fingerprints and physical significance. These conceptual underpinnings form the precursor to the main research target: first-principles study of pressure-induced topological phase transition in rare-earth compounds. The prime objective of this research is the investigation of yttrium monophosphide (YP) under hydrostatic pressure, employing hybrid density functional theory (DFT) to examine its structural, electronic, and topological evolution. In ambient conditions, YP is found to crystallize in a face-centered cubic (NaCl-type) structure and is a topologically trivial semimetal. Phonon dispersion and elastic constant calculations validate the dynamical and mechanical stability of this phase at high pressures. With increasing pressure, a topological phase transition occurs at 26.5 GPa, characterized by band inversion at the X -point and Dirac cone formation along the (001) plane. The \mathbb{Z}_2 invariant, obtained both from parity analysis at time-reversal invariant momenta and Wannier charge center evolution, changes from (0;000) to (1;000), testifying to the onset of a non-trivial topological phase. Furthermore, the material experiences a structure phase transition to another form at 63.6 GPa, again widening knowledge on pressure-induced behaviour in rare-earth monophosphides. This work thereby illustrates how outside pressure can function as an excellent tuning parameter for generating and governing topological behaviours in materials which otherwise remain trivial at usual states. The research

enhances the value of computational materials science in being able to foresee new quantum states and opens avenues for further experimental validation.

4.2. Future scope

The results of this dissertation provide the foundation for a number of intriguing future research directions. One step forward would be experimental confirmation of the theoretically predicted topological phase transition in YP under hydrostatic pressure. Methods like ARPES, high-pressure transport measurements, and X-ray diffraction would verify the band inversion and Dirac surface states, linking theoretical predictions to physical reality. Besides YP, the work can also be generalized to other rare-earth monpnictides which can show comparable or even more intricate topological behaviour under different external conditions of pressure, doping, or strain. A comparative study across these materials may show systematic trends and assist in determining key parameters that control topological phase transitions. Additionally, the inclusion of magnetism or external fields can result in new quantum phases, e.g. Weyl semimetals or magnetic topological insulators, thereby enriching research on topological materials. In applications, pressure tuneable topological materials show much potential towards next-generation electronic and spintronic devices. The existence of stable, non-dissipative surface states makes them prime prospects for energy-saving technologies. Further investigation into the effects of temperature and thermoelectric properties might also reveal their potential in energy conversion and thermal management. This work overall is a solid theoretical basis for designing and controlling new topological states and emphasizes pressure as a tool of great potency in quantum material engineering.

REFERENCES

-
- [1] E. H. Hall, On a New Action of the Magnet on Electric Currents, *Am. J. Sci.* 20 (1880) 287–292.
- [2] K. von Klitzing, G. Dorda, M. Pepper, New Method for High-Accuracy Determination of the Fine-Structure Constant Based on Quantized Hall Resistance, *Phys. Rev. Lett.* 45 (1980) 494–497.
- [3] D. J. Thouless, M. Kohmoto, M. P. Nightingale, M. den Nijs, Quantized Hall Conductance in a Two-Dimensional Periodic Potential, *Phys. Rev. Lett.* 49 (1982) 405–408.
- [4] C. L. Kane, E. J. Mele, \mathbb{Z}_2 Topological Order and the Quantum Spin Hall Effect, *Phys. Rev. Lett.* 95 (2005) 146802.
- [5] J. E. Moore, The birth of Topological insulators, *Nature* 464 (2010) 194.
- [6] M. Z. Hasan, J. E. Moore, Three-dimensional topological insulators, *Annu. Rev. Condens. Matter Phys.* 2 (2011) 55–78.
- [7] M. Z. Hasan, S.Y. Xu, M. Neupane, M. S. Roche, S. O. Valenzuela, Topological insulators, Topological Dirac semimetals, Topological Crystalline insulators and Topological Kondo insulators, (2015) arXiv:1604.08571.
- [8] X. L. Qi, S. C. Zhang, Topological insulators and superconductors, *Phys. Rev. Lett.* 83 (2011) 1057.
- [9] A. A. Burkov, Topological semimetals, *Nat. Mater.* 15 (2016) 1145–8.
- [10] X. Kong, L. Li, F. M. Peeters, Topological Dirac semimetal phase in Ge_xSn_y alloys, *Appl. Phys. Lett.* 112 (2018) 251601.
- [11] B. Singh, B. Ghosh, C. Su, H. Lin, A. Agarwal, A. Bansil, Topological Hourglass Dirac Semimetal in the Nonpolar Phase of Ag_2BiO_3 , *Phys. Phys. Lett.* 121 (2018) 226401.
- [12] A. Politano, G. Chiarello, B. Ghosh, K. Sadhukhan, C. N. Kuo, C. S. Lue, A. Agarwal, 3D Dirac Plasmons in the Type-II Dirac Semimetal, *Phys. Rev. Lett.* 121 (2018) 086804.
- [13] X. Wan, A. M. Turner, A. Vishwanath, S. Y. Savrasov, Topological semimetal and Fermi-arc surface states in the electronic structure of pyrochlore iridates, *Phys. Rev. B* 83 (2011) 205101.
- [14] H. Weng, C. Fang, Z. Fang, B. A. Bernevig, X. Dai, Weyl Semimetal Phase in Noncentrosymmetric Transition-Metal Monophosphides, *Phys. Rev. X* 5 (2015) 011029.
- [15] Z. K. Liu, L. X. Yang, Y. Sun, T. Zhang, H. Peng, H. F. Yang, Y. L. Chen, Evolution of the Fermi surface of Weyl semimetals in the transition metal pnictide family *Nat. Mater.* 15 (2016) 27–3.

- [16] B. Yan, C. Felser, Topological Materials: Weyl Semimetals, *Annu. Rev. Condens. Matter Phys.* 8 (2017) 337–354.
- [17] S.-Y. Xu, I. Belopolski, N. Alidoust, M. Neupane, G. Bian, C. Zhang, et al., Discovery of a Weyl Fermion Semimetal and Topological Fermi Arcs, *Science* 349 (2015) 613–617.
- [18] S. Murakami, N. Nagaosa, S.-C. Zhang, Dissipationless Quantum Spin Current at Room Temperature, *Science* 301 (2003) 1348–1351.
- [19] J. Sinova, D. Culcer, Q. Niu, N. A. Sinitsyn, T. Jungwirth, A. H. MacDonald, Universal Intrinsic Spin Hall Effect, *Phys. Rev. Lett.* 92 (2004) 126603.
- [20] L. Fu, C. L. Kane, Topological Insulators with Inversion Symmetry, *Phys. Rev. B* 76 (2007) 045302.
- [21] J. R. Munkres, *Topology*, 2nd ed., Prentice Hall, 2000.
- [22] L. Fu, Topological Crystalline Insulators, *Phys. Rev. Lett.* 106 (2011) 106802.
- [23] F. Schindler, A. M. Cook, M. G. Vergniory, Z. Wang, S. S. P. Parkin, B. A. Bernevig, T. Neupert, Higher-Order Topological Insulators, *Sci. Adv.* 4 (2018) eaat0346.
- [24] B. A. Bernevig, T. L. Hughes, S.-C. Zhang, Quantum Spin Hall Effect and Topological Phase Transition in HgTe Quantum Wells, *Science* 314 (2006) 1757–1761.
- [25] M. König, S. Wiedmann, C. Brüne, A. Roth, H. Buhmann, L. W. Molenkamp, X.-L. Qi, S.-C. Zhang, Quantum Spin Hall Insulator State in HgTe Quantum Wells, *Science* 318 (2007) 766–770.
- [26] L. Fu, C. L. Kane, E. J. Mele, Topological Insulators in Three Dimensions, *Phys. Rev. Lett.* 98 (2007) 106803.
- [27] H. Zhang, C.-X. Liu, X.-L. Qi, X. Dai, Z. Fang, S.-C. Zhang, Topological Insulators in Bi_2Se_3 , Bi_2Te_3 and Sb_2Te_3 with a Single Dirac Cone on the Surface, *Nat. Phys.* 5 (2009) 438–442.
- [28] Y. L. Chen et al., Experimental Realization of a Three-Dimensional Topological Insulator, Bi_2Te_3 , *Science* 325 (2009) 178–181.
- [29] Y. Xia, D. Qian, D. Hsieh, L. Wray, A. Pal, H. Lin, A. Bansil, D. Grauer, Y. S. Hor, R. J. Cava, M. Z. Hasan, Observation of a Large-Gap Topological-Insulator Class with a Single Dirac Cone on the Surface, *Nat. Phys.* 5 (2009) 398–402.
- [30] D. Hsieh, Y. Xia, D. Qian, L. Wray, J. H. Dil, F. Meier, J. Osterwalder, L. Patthey, J. G. Checkelsky, N. P. Ong, A. F. Vishwanath, M. Z. Hasan, Observation of Time-Reversal-Protected Single-Dirac-Cone Topological-Insulator States in Bi_2Te_3 and Sb_2Te_3 , *Phys. Rev. Lett.* 103 (2009) 146401.

- [31] S.-Y. Xu et al., Discovery of a Weyl Fermion Semimetal and Topological Fermi Arcs, *Science* 349 (2015) 613–617.
- [32] Z. Wang et al., Dirac Semimetal and Topological Phase Transitions in A_3Bi ($A=Na, K, Rb$), *Phys. Rev. B* 85 (2012) 195320.
- [33] Z. Wang et al., Three-dimensional Dirac semimetal and quantum transport in Cd_3As_2 , *Phys. Rev. B* 88 (2013) 125427.
- [34] S.-M. Huang et al., A Weyl Fermion semimetal with surface Fermi arcs in the transition metal monpnictide TaAs class, *Nat. Commun.* 6 (2015) 7373.
- [35] A. A. Burkov, M. D. Hook, L. Balents, Topological nodal semimetals, *Phys. Rev. B* 84 (2011) 235126.
- [36] N. P. Armitage, E. J. Mele, A. Vishwanath, Weyl and Dirac semimetals in three-dimensional solids, *Rev. Mod. Phys.* 90 (2018) 015001.
- [37] S. Murakami, Phase transition between the quantum spin Hall and insulator phases in 3D: emergence of a topological gapless phase, *New J. Phys.* 9 (2007) 356.
- [38] A. M. Turner, A. Vishwanath, Beyond Band Insulators: Topology of Semi-metals and Interacting Phases, *arXiv:1301.0330* (2013).
- [39] H. Lin et al., Half-Heusler ternary compounds as new multifunctional experimental platforms for topological quantum phenomena, *Nat. Mater.* 9 (2010) 546–549.
- [40] C.-C. Lee, C.-Y. Huang, C.-H. Hsu, Topological phase transitions in semimetals, *J. Phys. Condens. Matter* 31 (2019) 183001.
- [41] Manzoni, G., et al., Evidence for a Strong Topological Insulator Phase in $ZrTe_5$, *Physical Review Letters*, 117 (2016) 237601.
- [42] Lu, Y., et al., Topological phase transition in $HfTe_5$ induced by temperature, *Physical Review B*, 95 (2017) 014201.
- [43] Q. D. Gibson et al., Three-dimensional Dirac semimetals: Design principles and predictions of new materials, *Phys. Rev. B* 91 (2015) 205128.
- [44] T. Liang et al., Anomalous Hall effect in $ZrTe_5$, *Nat. Phys.* 14 (2018) 451–455.
- [45] Y. Zhang et al., Electronic evidence of temperature-induced Lifshitz transition and topological nature in $ZrTe_5$, *Nat. Commun.* 8 (2017) 15512.
- [46] L. Moreschini et al., Electronic structure of the candidate type-II Weyl semimetal WTe_2 , *Phys. Rev. B* 95 (2017) 121101.
- [47] S. Wu et al., Observation of Fermi arcs in the type-II Weyl semimetal candidate WTe_2 , *Science* 349 (2015) 6248.

- [48] G. Kresse, J. Furthmüller, Efficient iterative schemes for ab initio total-energy calculations using a plane-wave basis set, *Phys. Rev. B* 54 (1996) 11169.
- [49] A. A. Mostofi, J. R. Yates, Y.-S. Lee, I. Souza, D. Vanderbilt, N. Marzari, Wannier90: A tool for obtaining maximally-localised Wannier functions, *Comput. Phys. Commun.* 178 (2008) 685.
- [50] Q. Wu, S. Zhang, H.-F. Song, M. Troyer, A. A. Soluyanov, WannierTools: An open-source software package for novel topological materials, *Comput. Phys. Commun.* 224 (2018) 405.
- [51] W. Kohn, L. J. Sham, Self-consistent equations including exchange and correlation effects, *Phys. Rev.* 140 (1965) A1133.
- [52] J. P. Perdew, K. Burke, M. Ernzerhof, Generalized Gradient Approximation Made Simple, *Phys. Rev. Lett.* 77 (1996) 3865.
- [53] J. Heyd, G. E. Scuseria, M. Ernzerhof, Hybrid functionals based on a screened Coulomb potential, *J. Chem. Phys.* 118 (2003) 8207.
- [54] Q. Wu, S. Zhang, H.-F. Song, M. Troyer, A. A. Soluyanov, WannierTools: An open-source software package for novel topological materials, *Comput. Phys. Commun.* 224 (2018) 405.
- [55] M. Z. Hasan, C. L. Kane, Colloquium: Topological Insulators, *Rev. Mod. Phys.* 82 (2010) 3045–3067.
- [56] M. Hirayama, R. Okugawa, S. Murakami, Topological Semimetals Studied by Ab Initio Calculations *J. Phys. Soc. Japan* 87 (2018) 041002.
- [57] P. J. Guo, H. C. Yang, Liu and Z. Y. Lu, Theoretical study of the pressure-induced topological phase transition in LaSb, *Phys. Rev. B* 96 (2017) 081112
- [58] S. Khalid, F. P. Sabino, A. Janotti, Topological phase transition in LaAs under pressure, *Phys. Rev. B* 98 (2018) 220102.
- [59] R. Lou, B. B. Fu, Q. N. Xu, P. J. Guo, L. Y. Kong, L. K. Zeng, S. C. Wang, Evidence of topological insulator state in the semimetal LaBi, *Phys. Rev. B* 95 (2017) 115140.
- [60] X. Duan, F. Wu, J. Chen, P. Zhang, Y. Liu, H. Yuan, C. Cao, Tunable electronic structure and topological properties of LnPn (Ln=Ce, Pr, Sm, Gd, Yb; Pn=Sb, Bi), *Commun. Phys.* 1 (2018) 71.
- [61] J. Nayak, S. C. Wu, N. Kumar, C. Shekhar, S. Singh, J. Fink, C. Felser, Multiple Dirac cones at the surface of the topological metal LaBi, *Nat. Commun.* 8 (2017) 13942.

- [62] Z. K. Liu, L. X. Yang, S. C. Wu, C. Shekhar, J. Jiang, H. F. Yang, Y. L. Chen, Observation of unusual topological surface states in half-Heusler compounds LnPtBi ($\text{Ln}=\text{Lu}, \text{Y}$), *Nat. Commun.* 7 (2016) 12924.
- [63] M. Zeng, C. Fang, G. Chang, Y. A. Chen, T. Hsieh, A. Bansil, L. Fu, Topological semimetals and topological insulators in rare earth monpnictides, (2015) arXiv:1504.03492.
- [64] C. Guo, C. Cao, M. Smidman, F. Wu, Y. Zhang, F. Steglich, H. Yuan, Possible Weyl fermions in the magnetic Kondo system CeSb , *NPJ Quantum Mater.* 2 (2017) 39.
- [65] N. Alidoust et al, A new form of (unexpected) Dirac fermions in the strongly-correlated cerium monpnictides, (2016) arXiv:1604. 08571.
- [66] K. Kuroda et al, Experimental Determination of the Topological Phase Diagram in Cerium Monpnictides, *Phys. Rev. Lett.* 120 (2018) 086402.
- [67] P. Li, Z. Wu, F. Wu, C. Cao, C. Guo, Y. Wu, Y. Liu, Tunable electronic structure and surface states in rare-earth monobismuthides with partially filled shell, *Phys. Rev. B* 98 (2018) 085103.
- [68] Nidhi, R. Kumar, R. K Bibiyan and M. Singh, Emergence of topological phase and non-trivial surface states in rare-earth semimetal GdSb with pressure, *J. Phys. D: Appl. Phys.* 58 (2025) 015304.
- [69] P. Wadhwa, S. Kumar, A. Shukla, R. Kumar, First principles investigation of topological phase in XMR material TmSb under hydrostatic pressure, *J. Condens. Matter Phys.* 31 (2019) 335401.
- [70] R. Kumar, M. Singh, Appearance of topological phase in YAs semimetal under hydrostatic pressure and epitaxial strain, *Journal of Physics and Chemistry of Solids* 196 (2025) 112356.
- [71] P. Wadhwa, R. Kumar, S. Kumar, A. Shukla, Studies of non-trivial band topology and electron-hole compensation in YSb , *Solid State Commun.* 321 (2020) 114022.
- [72] R. Kumar, M. Singh, Topological phase transition and tunable surface states in YBi *J. Phys.: Condens. Matter* 36 (2024) 345601.
- [73] M. Singh, R. Kumar, R. K Bibiyan, Pressure-induced topological phase transition in XMR material YbAs : a first-principles study, *Eur. Phys. J. Plus* 137 (2022) 633.
- [74] P. Bhardwaj, S. Singh, Structural, mechanical and thermo physical properties of III–V yttrium pnictides with NaCl -structure under high pressure, *Mat. Chem. and Phys.* 125 (2011) 440–448.
- [75] B. Amrani, F. E. H. Hassan, Theoretical study of III–V yttrium compounds, *Computational Materials Science* 39 (2007) 563–568.

- [76] F. Soyalp, S. Uğur, Structural, electronic and phonon properties investigation of YP and YAs compounds, *J. Phys. Chem. Solids* 69 (2008) 791–798.
- [77] N. Kaurav, Y. K. Kuo, G. Joshi, K. K. Choudhary, D. Varshney, High-pressure structural phase transition and elastic properties of yttrium pnictides, *High Press. Res.* 28 (4) (2008) 651–663.
- [78] A. Singh, V. Srivastava, M. Aynyas, S .P. Sanyal, High pressure structural phase transition and elastic properties of yttrium pnictides, *Physica B* 404 (2009) 1852–1857.
- [79] A. Bouhemadou, Elastic constants and high pressure structural transitions in yttrium pnictides, *Comp. Mater. Sci.* 43 (2008) 1112–1116.
- [80] P. Hohenberg, W. Kohn, Inhomogeneous Electron Gas, *Phys. Rev.* 136 (1964) B864.
- [81] W. Kohn, L. J. Sham, Self-Consistent Equations Including Exchange and Correlation Effects, *Phys. Rev.* 140 (1965) A1133.
- [82] G. Kresse, D. Joubert, From ultrasoft pseudopotentials to the projector augmented-wave method, *Phys. Rev. B* 59 (1999) 1758.
- [83] H. J. Monkhorst, J. D. Pack, Special points for Brillouin-zone integrations, *Phys. Rev. B* 13 (1976) 5188–5192.
- [84] A. Togo, First-principles Phonon Calculations with Phonopy and Phono3py, *J. Phys. Soc. Jpn.* 92 (2023) 012001-1-21.
- [85] V. Wang, N. Xu, J. C. Liu, G. Tang, W. T. Geng, VASPKIT: A User-Friendly Interface Facilitating High-Throughput Computing and Analysis Using VASP Code, *Comp. Phys. Comm.* 267 (2021) 108033.
- [86] Z. J. Wu, E. J. Zhao, H. P. Xiang, X. F. Hao, X. J. Liu, J. Meng, Crystal structures and elastic properties of superhard IrN₂ and IrN₃ from first principles, *Phys. Rev. B* 76 (2007) 54115–54129.
- [87] Hirohata, A., Yamada, K., Nakatani, Y., Hillebrands, B., Review on Spintronics: Principles and Device Applications, *Journal of Magnetism and Magnetic Materials*, 509 (2020) 166711.
- [88] Wen, C., Lui, L. M., Geometric Registration of High-Genus Surfaces, *IEEE Transactions on Image Processing*, 22 (2013) 5046–5059.
- [89] Topological Insulators: Bridging Quantum Physics and Geometry, Exploring the Unique Properties of Materials That Conduct Electricity at Their Edges While Insulating in the Bulk
- [90] B. Yan, C. Felser, Topological Materials: Weyl Semimetals, *Annual Review of Condensed Matter Physics*, 8 (2017) 337–354.

PLAGIARISM REPORT



Page 1 of 57 - Cover Page

Submission ID trn:oid:::27535:99322999

Anushka_Thesis.docx

 Delhi Technological University

Document Details

Submission ID

trn:oid:::27535:99322999

Submission Date

Jun 4, 2025, 5:37 PM GMT+5:30

Download Date

Jun 8, 2025, 11:06 AM GMT+5:30

File Name

Final Thesis_editedd.docx

File Size

5.1 MB

51 Pages

12,205 Words

67,746 Characters



Page 1 of 57 - Cover Page

Submission ID trn:oid:::27535:99322999

9% Overall Similarity

The combined total of all matches, including overlapping sources, for each database.

Filtered from the Report

- Bibliography
- Quoted Text
- Cited Text
- Small Matches (less than 10 words)

Exclusions

- 1 Excluded Source
- 22 Excluded Matches

Match Groups

- 76 Not Cited or Quoted 9%**
Matches with neither in-text citation nor quotation marks
- 0 Missing Quotations 0%**
Matches that are still very similar to source material
- 0 Missing Citation 0%**
Matches that have quotation marks, but no in-text citation
- 0 Cited and Quoted 0%**
Matches with in-text citation present, but no quotation marks

Top Sources

- 5% Internet sources
- 7% Publications
- 4% Submitted works (Student Papers)

Integrity Flags

0 Integrity Flags for Review

No suspicious text manipulations found.

Our system's algorithms look deeply at a document for any inconsistencies that would set it apart from a normal submission. If we notice something strange, we flag it for you to review.

A Flag is not necessarily an indicator of a problem. However, we'd recommend you focus your attention there for further review.

Aughke

Rashmi

[Signature]

Match Groups

- 76 Not Cited or Quoted 9%**
Matches with neither in-text citation nor quotation marks
- 0 Missing Quotations 0%**
Matches that are still very similar to source material
- 0 Missing Citation 0%**
Matches that have quotation marks, but no in-text citation
- 0 Cited and Quoted 0%**
Matches with in-text citation present, but no quotation marks

Top Sources

- 5%** Internet sources
- 7%** Publications
- 4%** Submitted works (Student Papers)

Top Sources

The sources with the highest number of matches within the submission. Overlapping sources will not be displayed.

1	Publication	Ramesh Kumar, Mukhtiyar Singh. "Appearance of topological phase in YAs semi...	1%
2	Publication	Nidhi, Ramesh Kumar, Ramesh K Bibiyan, Mukhtiyar Singh. "Emergence of topolo...	<1%
3	Publication	Ramesh Kumar, Rajesh Kumar, Antik Sihi, Mukhtiyar Singh. "Unraveling the topol...	<1%
4	Publication	Khanna, Ajay. "Modeling Optical Spectroscopy and Resonance Energy Transfer fo...	<1%
5	Internet	www.researchgate.net	<1%
6	Internet	iopscience.iop.org	<1%
7	Internet	export.arxiv.org	<1%
8	Publication	Ramesh Kumar, Mukhtiyar Singh. "Topological phase transition and tunable surf...	<1%
9	Submitted works	Addis Ababa University on 2024-09-10	<1%
10	Publication	Ramesh Kumar, Mukhtiyar Singh. "Existence of dual topological phases in Sn-bas...	<1%



Contents lists available at ScienceDirect

Physics Letters A

journal homepage: www.elsevier.com/locate/pla

Letter

An *ab-initio* study of structural and topological phase transition in rare-earth yttrium monophosphide

Anushka Pal, Rashmi Yadav, Ramesh Kumar , Mukhtiyar Singh

Computational Quantum Materials Design (CQMD) Lab, Department of Applied Physics, Delhi Technological University, Delhi 110042, India

ARTICLE INFO

Communicated by Lilla Woods

Keywords:

Topological phase transition
Rare earth monophosphides
First-principles calculations
VASP
Hybrid functional

ABSTRACT

The rare-earth monophosphide materials exhibiting topological properties have attracted considerable attention of condensed matter physicists. This article utilizes hybrid density functional theory to examine the structural stability, electronic properties, and topological phase characteristics of the rare-earth semimetal yttrium monophosphide (YP) when subjected to hydrostatic pressure. This material exhibits a stable face-centered cubic (NaCl-type) structure, which undergoes a structural phase transition at a hydrostatic pressure of 63.6 GPa. It is a topologically trivial semimetal at ambient pressure but shows a topological phase transition at 26.5 GPa pressure. The topologically non-trivial phase in this material is substantiated via the band inversion at the *X*-point and the existence of the Dirac cone along the (001) plane. The product of parities at time-reversal invariant momenta points and the evolution of Wannier charge centers are used to calculate the \mathbb{Z}_2 topological invariants and obtain the values (1; 000) at 26.5 GPa.

1. Introduction

The investigation of topological phenomena has emerged as one of the most important areas of research in the field of condensed matter physics in recent years [1–4]. The Topological materials (TMs) have an unusual conducting quantum state at the surface/edge but an insulating nature in bulk [3,4]. These conducting surface states are doubly protected by time-reversal symmetry (TRS) as well as inversion symmetry (IS) and are robust against impurities and defects [5–7]. Spin-orbit coupling (SOC) plays an important role in TMs [1–3]. These materials are identified as topologically non-trivial due to the presence of topological surface states (TSSs) and can be characterized by the \mathbb{Z}_2 topological invariants. These TMs can further divide into topological insulators (TIs) [4,6–8], topological crystalline insulators (TCIs) [7], topological semimetals (TSMs) [9–12], etc. The TSMs can be categorized into Dirac semimetals (DSMs) [12], Weyl semimetals (WSMs), [11], and node-lines semimetals (NLSMs) [13–15], etc., depending upon the symmetry protection and nature of TSSs. For example, a DSM can be converted into WSM if either TRS or IS is broken [16]. These semimetals have a crossing of the valence band (VB) and the conduction band (CB) at some isolated momenta points in the Brillouin zone (BZ) and a clear gap in eigenstates near the Fermi energy elsewhere. There exist another class of TSMs known as \mathbb{Z}_2 topological semimetals, which have a

localized energy band gap in the momentum space and TSS in these materials is protected by TRS as well as IS [17,18]. The \mathbb{Z}_2 topological semimetals have been realized in rare-earth monophosphides (RE-M); RE: rare-earth elements and M: pnictide elements [19–23]. Several RE-M (RE=Ce, La, Pr, Sm, Gd, Yb; M= Bi, Sb, As, P) have been reported to exhibit topologically semimetallic band structures at ambient pressure [19–23]. The angle-resolved photoemission spectroscopy (ARPES) studies of CeSb and CeBi semimetals [24,25] and *first-principles* investigations of CeSb, CeBi, PrSb, PrBi, SmBi, and GdBi have been reported the topological phases in these materials [20,25–27].

It has been observed that the topological phase transition (TPT) can be induced in RE-M materials via hydrostatic pressure, without disturbing the charge neutrality and the stoichiometry of these materials. The RE-M materials such as LaSb [17], GdSb [28], LaAs [18], TmSb [29], YX (X= As, Sb, Bi) [30–32], and YbAs [33,34] have shown the TPT from trivial to non-trivial topological phase under the applied hydrostatic pressure. The non-magnetic YX (X= N, P, As, Sb, Bi) materials also belong to the RE-M family and their structural stability has been reported over a large range of hydrostatic pressure [36–39]. These materials are semimetallic, and it has been shown that the YAs, YSb and YBi exhibit TPT under hydrostatic pressure and epitaxial strain [30–32]. Another member of this family, i.e., Yttrium monophosphide (YP), also has a semimetallic nature and structural stability at relatively higher

* Corresponding author.

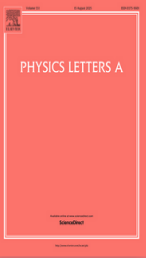
E-mail address: mukhtiyarsingh@dtu.ac.in (M. Singh).<https://doi.org/10.1016/j.physleta.2025.130650>

Received 15 February 2025; Received in revised form 8 May 2025; Accepted 13 May 2025

Available online 14 May 2025

0375-9601/© 2025 Elsevier B.V. All rights are reserved, including those for text and data mining, AI training, and similar technologies.

PROOF AND SCOPUS INDEXING



Physics Letters A

Supports open access

5.1

CiteScore

2.3

Impact Factor

Articles & Issues ▾

About ▾

Publish ▾

Order journal ↗

 Search in this journal

Submit your article ↗

Guide for authors

PHYSICS LETTERS A

Publisher: ELSEVIER , RADARWEG 29, AMSTERDAM, Netherlands, 1043 NX

ISSN / eISSN: 0375-9601 / 1873-2429

Web of Science Core Collection: Science Citation Index Expanded

Additional Web of Science Indexes: Current Contents Physical, Chemical & Earth Sciences | Essential Science Indicators

 Share This Journal

[View profile page](#)

* Requires free login.

LIST OF CONFERENCE

Name of Conference: International Conference on Emerging Materials and Quantum Photonics (ICEMQP-2024)

Conference Dates: 2024, November 7-9

Mode of the Conference: Offline

Venue: Guru Jambheshwar University of Science and Technology, Hisar, Haryana, India

PARTICIPATION RECORD

